NFκB1 is essential to prevent the development of multiorgan autoimmunity by limiting IL-6 production in follicular B cells

Elisha de Valle,[1,2] George Grigoriadis,[3,6,7]* Lorraine A. O'Reilly,[8,9]* Simon N. Willis,[8,9] Mhairi J. Maxwell,[2] Lynn M. Corcoran,[8,9] Evelyn Tsantikos,[2] Jasper K.S. Cornish,[1,2] Kirsten A. Fairfax,[8,9] Ajithkumar Vasanthakumar,[8,9] Mark A. Febbraio,[10] Margaret L. Hibbs,[2] Marc Pellegrini,[8,9] Ashish Banerjee,[6] Philip D. Hodgkin,[8,9] Axel Kallies,[8,9] Fabienne Mackay,[2] Andreas Strasser,[8,9] Steve Gerondakis,[4,5] and Raffi Gugasyan[1,2]

[1]Burnet Institute, Melbourne, VIC 3004, Australia
[2]Immunology, Central Clinical School, [3]School of Clinical Sciences, [4]Infection and Immunity Program, Monash Biomedical Discovery Institute, and [5]Department of Biochemistry and Molecular Biology, Monash University, Melbourne, VIC 3004, Australia
[6]Center for Cancer Research, Hudson Institute of Medical Research, Melbourne, VIC 3168, Australia
[7]Clinical Haematology, Monash and Alfred Health, Melbourne, VIC 3168, Australia
[8]Walter and Eliza Hall Institute of Medical Research, Melbourne, VIC 3052, Australia
[9]Department of Medical Biology, University of Melbourne, Melbourne, VIC 3050, Australia
[10]Garvan Institute of Medical Research, Darlinghurst, Sydney, NSW 2010, Australia

We examined the role of NFκB1 in the homeostasis and function of peripheral follicular (Fo) B cells. Aging mice lacking NFκB1 (*Nfκb1*$^{-/-}$) develop lymphoproliferative and multiorgan autoimmune disease attributed in large part to the deregulated activity of *Nfκb1*$^{-/-}$ Fo B cells that produce excessive levels of the proinflammatory cytokine interleukin 6 (IL-6). Despite enhanced germinal center (GC) B cell differentiation, the formation of GC structures was severely disrupted in the *Nfκb1*$^{-/-}$ mice. Bone marrow chimeric mice revealed that the Fo B cell–intrinsic loss of NFκB1 led to the spontaneous generation of GC B cells. This was primarily the result of an increase in IL-6 levels, which promotes the differentiation of Fo helper CD4^{+} T cells and acts in an autocrine manner to reduce antigen receptor and toll-like receptor activation thresholds in a population of proliferating IgM^{+} *Nfκb1*$^{-/-}$ Fo B cells. We demonstrate that p50-NFκB1 represses *Il-6* transcription in Fo B cells, with the loss of NFκB1 also resulting in the uncontrolled RELA-driven transcription of *Il-6*. Collectively, our findings identify a previously unrecognized role for NFκB1 in preventing multiorgan autoimmunity through its negative regulation of *Il-6* gene expression in Fo B cells.

Follicular (Fo) B cells play an essential role in T cell–dependent immunity and plasma cell and memory B cell generation (Pillai et al., 2011). Antigen-specific B cell activation leads to plasma cell and memory B cell development in specialized compartments called germinal centers (GCs). Antigen encounter, together with cognate T helper cells and critical cytokines, including IL-6 and IL-21, promotes the formation of GCs (Klein and Dalla-Favera, 2008). Within GCs, B cells undergo extensive proliferation accompanied by Ig V gene somatic hypermutation and isotype switching. This process occurs when B cells engage CD4^{+} Fo T helper cells (T_{FH} cell; Crotty, 2011; Ueno et al., 2015). Through direct cell contact and IL-6 production, B cells induce T_{FH} cell differentiation, which in turn promotes the proliferation of GC B cells through the secretion of IL-21, culminating in the formation of extra-Fo Ab-secreting cells (Nurieva et al., 2008; Crotty, 2011). Although B cell activation and GC formation is critical for generating long-term humoral immunity, deregulated GC responses are intimately associated with human diseases, including systemic lupus erythematosus and lymphomas (Vinuesa et al., 2009; Shaffer et al., 2012).

The NFκB signaling pathway plays essential roles in inflammation and cell survival, differentiation, and proliferation (Gerondakis and Siebenlist, 2010; de Valle et al., 2012). NFκB transcription factors are comprised of homo- and heterodimers of RELA, c-REL, and RELB, which have transcriptional transactivation domains. However, p50-NFκB1 and p52-NFκB2, derived from their respective precursors p105 and p100, lack intrinsic transactivating properties and

*G. Grigoriadis and L.A. O'Reilly contributed equally to this paper.

Correspondence to Raffi Gugasyan: gugasyan@burnet.edu.au

Abbreviations used: Ab, antibody; ANA, antinuclear auto-Ab; BCR, B cell receptor; ChIP, chromatin immunoprecipitation; ERK, extracellular signal–regulated protein kinase; Fo, follicular; GC, germinal center; IKK, IκB kinase; mBM, mixed BM; MZ, marginal zone; qPCR, quantitative PCR.

The Rockefeller University Press $30.00
J. Exp. Med. 2016 Vol. 213 No. 4 621–641
www.jem.org/cgi/doi/10.1084/jem.20151182

generally induce gene expression when paired with RELA, c-REL, and RELB (Hayden and Ghosh, 2011). Conversely, p50-NFκB1 and p52-NFκB2 homodimers function as transcriptional repressors or, in certain instances, as inducers of gene expression when partnered with transcriptional coactivators (Hayden and Ghosh, 2011). In most cells, the majority of transactivation-competent NFκB heterodimers are retained in an inactive state within the cytoplasm by IκB proteins. Stimuli, including cytokines, activate an upstream IκB kinase (IKK; αβγ subunits) complex, which phosphorylates IκB proteins, targeting them for proteasome-mediated degradation (Hayden and Ghosh, 2011). NFκB heterodimers then translocate to the nucleus and regulate transcription by binding to κB elements within regulatory regions of target genes.

NFκB signaling regulates key roles in B cell development, activation, and function (Kaileh and Sen, 2012). Noncanonical NFκB signaling generates p52-NFκB2 by p100-NFκB2 processing, with IKK-α– and NFκB2-deficient mice showing impaired BAFF-driven survival of immature B cells and defective CD40-mediated B cell activation (Claudio et al., 2002; Kaileh and Sen, 2012). The conditional deletion of IKK-β or -γ reveals a cell-intrinsic requirement for the canonical pathway in mature B cells, manifested as a dramatic reduction in peripheral B cell numbers (Pasparakis et al., 2002; Li et al., 2003; Jacque et al., 2014). The most abundant NFκB proteins in mature Fo B cells are p50/c-REL plus p50/RELA heterodimers and p50 homodimers (Grumont and Gerondakis, 1994). Although B cell receptor (BCR), TLR, and CD40 signals all rapidly activate NFκB signaling, the high levels of p50 homodimers that reside in the nuclei of resting B cells serve an unknown role. The c-REL subunit is required for the activation of mature B cells, controlling cell cycle progression, cell survival, and isotype switching (Grumont et al., 1998; Cheng et al., 2003). Although p50-NFκB1 cooperates with c-REL to regulate B cell activation (Grumont et al., 2002; Pohl et al., 2002), much less is known about its nonredundant role in mature Fo B cells. Young *Nfκb1*$^{-/-}$ mice display several B cell defects, including reduced numbers of transitional and marginal zone (MZ) B cells, enhanced Fo B cell turnover, and defects in Ig class switching (Sha et al., 1995; Snapper et al., 1996; Cariappa et al., 2000). This is in part the result of the distinct roles served by p50 and p105, both of which are absent in *Nfκb1*$^{-/-}$ mice. p105-NFκB1 regulates extracellular signal–regulated protein kinase (ERK) signaling through its interaction with the MEK1/2 kinase Tpl2 (Beinke et al., 2003; Waterfield et al., 2003). In *Nfκb1*$^{-/-}$ mice, Tpl-2 is rapidly degraded, resulting in impaired ERK activity (Waterfield et al., 2003), which, in B cells, contributes to defects in TLR4-induced activation (Banerjee et al., 2008).

In this study, we report a critical role for p50-NFκB1 in peripheral B cell homeostasis. Aging *Nfκb1*$^{-/-}$ mice were shown to develop lymphoproliferative and multiorgan autoimmune disease. Using BM chimeric mice, we demonstrate that the absence of NFκB1 in Fo B cells elicits aberrant B cell proliferation and differentiation that culminates in the development of autoimmune pathologies. Fo B cells lacking NFκB1 spontaneously produce IL-6, which drives disease pathogenesis. Autocrine IL-6/IL-6R signaling was found to lower the BCR and TLR activation threshold in a population of proliferating IgM^{hi} *Nfκb1*$^{-/-}$ Fo B cells, whereas the enhanced production of IL-6 acts in a paracrine manner to promote excessive T_{FH} cell differentiation that results in the accumulation of GC B cells in *Nfκb1*$^{-/-}$ mice. Collectively, our data reveal an essential negative regulatory role for NFκB1 in Fo B cells that prevents the spontaneous development of autoimmune disease.

RESULTS

Aging *Nfκb1*$^{-/-}$ mice develop multiorgan autoimmune pathology

Consistent with recent studies (Bernal et al., 2014; Jurk et al., 2014), mice lacking *Nfκb1* (*Nfκb1*$^{-/-}$) housed in conventional or barrier airflow conditions have a significantly reduced lifespan compared with WT mice on the same genetic (C57BL/6) background (median survival of *Nfκb1*$^{-/-}$ mice [587 d] vs. WT mice [860 d]). Despite a normal appearance up to 1 yr of age, *Nfκb1*$^{-/-}$ mice subsequently displayed cachexia that necessitated euthanasia. At necropsy (453 ± 101 d), *Nfκb1*$^{-/-}$ mice exhibited multiorgan immune infiltrates affecting the lungs, liver, salivary glands, pancreas, gastrointestinal tract, and kidney (not depicted). The kidneys from 53-wk-old *Nfκb1*$^{-/-}$ mice also showed a low incidence of glomerulonephritis, indicating that these mice developed autoimmune disease. To explore this further, we measured serum Ig levels and screened for auto-Abs. Basal IgM levels were elevated approximately threefold in 20-wk-old *Nfκb1*$^{-/-}$ mice compared with WT controls, whereas other Ig isotypes were significantly reduced (IgG_1, IgG_{2b}, and IgG_{2c}) or normal (IgA; Fig. 1 A). Reduced IgG_{2b} levels are likely the result of impaired isotype switching, which requires NFκB1 (Snapper et al., 1996). Aged *Nfκb1*$^{-/-}$ mice also had auto-Abs to organs, including the stomach, lungs, pancreas, and salivary glands (Fig. 1 B). These data demonstrate that the reduced lifespan of *Nfκb1*$^{-/-}$ mice is associated with the development of multiorgan autoimmune disease.

Abnormally increased numbers of T_{FH} and GC B cells in aged *Nfκb1*$^{-/-}$ mice

The presence of auto-Abs prompted the examination of lymphoid cells in aging *Nfκb1*$^{-/-}$ mice. Like young *Nfκb1*$^{-/-}$ mice (6–10 wk), the B cell transition from T1 to T2 was impaired, and MZ B cell numbers were markedly reduced in 40-wk-old *Nfκb1*$^{-/-}$ mice (Fig. 1 C). However, although young *Nfκb1*$^{-/-}$ mice contained normal numbers of naive Fo B cells, aged *Nfκb1*$^{-/-}$ mice developed splenomegaly, primarily because of increased numbers of activated Fo B cells (Fig. 1, C and D). We extended our analysis to include GC B cells ($B220^+FAS^+GL\text{-}7^+$), which gradually accumulate in the spleens of aging WT mice (Fig. 1 E). The number of GC B cells was significantly reduced in young *Nfκb1*$^{-/-}$ mice but consistently higher in the older *Nfκb1*$^{-/-}$ mice (Fig. 1 E).

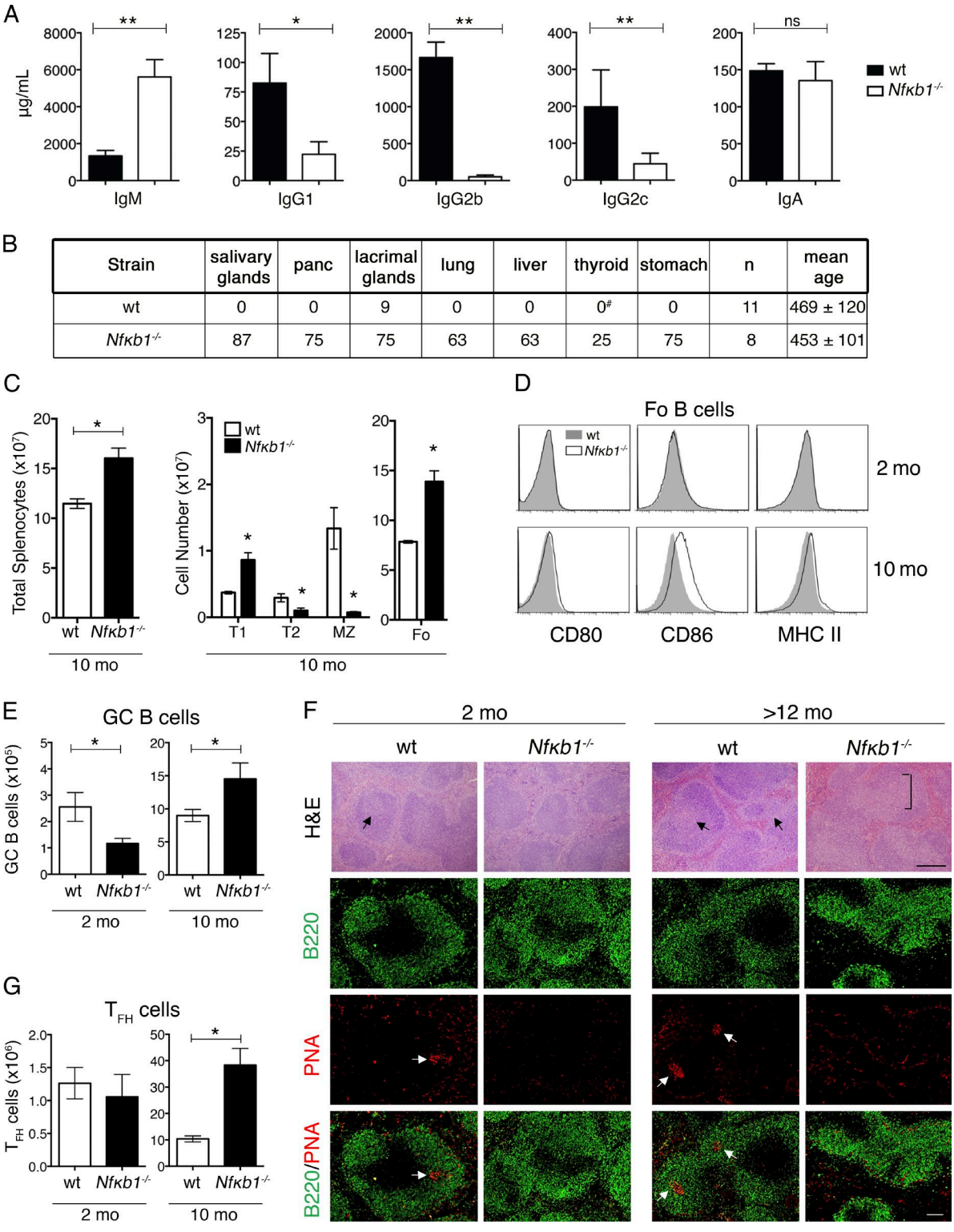

Strain	salivary glands	panc	lacrimal glands	lung	liver	thyroid	stomach	n	mean age
wt	0	0	9	0	0	0#	0	11	469 ± 120
Nfκb1$^{-/-}$	87	75	75	63	63	25	75	8	453 ± 101

Figure 1. **Aged *Nfκb1*$^{-/-}$ mice develop multiorgan autoimmune disease.** (A) Serum Ig levels in 5-mo-old WT and *Nfκb1*$^{-/-}$ mice measured by ELISA (n = 6 mice/genotype). (B) Mice with organ-specific auto-Abs (percentage incidence). Tissue cryosections from *rag-1/J* mice were stained with sera from aged or sick mice and detected by goat anti–mouse Ig-FITC (as shown in Fig 2 D). #, n = 5. (C–E) Flow cytometric analysis of splenic B cell subsets in WT and *Nfκb1*$^{-/-}$ mice (C). Absolute cell numbers of T1 (CD23^{-}B220^{+}CD21^{lo}), T2 (CD23^{+}B220^{+}CD21^{hi}), MZ (CD23^{-}B220^{+}CD21^{hi}), and Fo (CD23^{+}B220^{+}CD21^{lo}) B cells. (D) Cell surface markers in WT and *Nfκb1*$^{-/-}$ Fo B cells. (E) Absolute numbers of GC B cells (B220^{+}FAS^{+}GL7^{+}). (F) H&E-stained splenic sections (top). Two-color

Regardless of age, *Nfκb1*$^{-/-}$ GC B cells expressed less membrane-bound FAS and GL-7 (Fig. S1 A). To establish whether GC structures in the spleens of *Nfκb1*$^{-/-}$ mice were normal, we initially examined hematoxylin and eosin (H&E)–stained sections. Although small GCs were observed in young WT mice, these were not detected in the *Nfκb1*$^{-/-}$ mice (Fig. 1 F). As reported recently (Jurk et al., 2014), there were large atypical GC-like structures in the spleens of the aged *Nfκb1*$^{-/-}$ mice. Staining with anti-B220 Ab and PNA lectin, a specialized GC marker, revealed that the spleens of both young and aging *Nfκb1*$^{-/-}$ mice were devoid of GC structures (Fig. 1 F). Thus, the phenotypic differences displayed by *Nfκb1*$^{-/-}$ GC B cells coincide with a failure to form bona fide GC structures in *Nfκb1*$^{-/-}$ mice.

Because excess numbers of T_{FH} cells can increase the generation of GC B cells (Ueno et al., 2015), we examined T_{FH} cell development in *Nfκb1*$^{-/-}$ mice. Based on the characteristic T_{FH} cell surface markers CXCR5, PD-1, and ICOS, young WT and *Nfκb1*$^{-/-}$ mice had comparably low numbers of T_{FH} cells (Figs. 1 G and S1 B). However, compared with age-matched WT mice, an approximately threefold increase in T_{FH} cell numbers was observed in old *Nfκb1*$^{-/-}$ mice (Fig. 1 G). Overall, these results are consistent with NFκB1 curtailing the production of T_{FH} and GC B cells.

Absence of NFκB1 in hematopoietic cells leads to aberrant lymphoproliferation and multiorgan autoimmune disease

To establish whether the aforementioned abnormalities are the result of a loss of NFκB1 within the stromal or hematopoietic compartments, we used BM chimera mice. Engraftment of WT BM into lethally irradiated *Nfκb1*$^{-/-}$ hosts did not lead to multiorgan inflammation or splenomegaly, and the distribution of lymphoid cells was normal (Fig. 2, A and B; and Fig. 3 A). In marked contrast, irradiated ly5.1^{+} WT mice that received *Nfκb1*$^{-/-}$ BM presented with a phenotype resembling aged *Nfκb1*$^{-/-}$ mice but with a significantly accelerated disease onset. These chimeras displayed abdominal swelling at 6–8 mo after reconstitution and, at autopsy, displayed splenomegaly and lymphadenopathy (Fig. 2 A). Histological analysis confirmed the presence of multiorgan immune infiltrates (Fig. 2 B, left), although gastrointestinal pathology and glomerulonephritis were not detected. Affected organs displayed a perivascular lymphoid infiltrate (Fig. 2 B, left and top right), and tissue integrity was preserved in most organs, with the exception of exocrine acinar cell destruction in the pancreas (Fig. 2 B, bottom right). The lymphoid infiltrate in the pancreas was confined to exocrine tissue, and in severe cases, only islet cells were preserved (Fig. 2 B, bottom right). Overall, ∼98% (39/40) of hosts injected with *Nfκb1*$^{-/-}$ BM displayed multiorgan inflammation.

Mice engrafted with *Nfκb1*$^{-/-}$ BM also had an altered serum Ig profile (Fig. 2 C). IgM levels were significantly elevated, whereas IgG_1 and IgG2c, which were markedly reduced in the aged *Nfκb1*$^{-/-}$ mice, were detected at high to normal levels. IgG_{2b} levels, however, were significantly reduced in both mouse models. The sera of these chimeric mice also contained auto-Abs to the liver, epithelial cells in the lungs, and, most commonly, the pancreas and salivary and lacrimal glands (Fig. 2 D, left and top right). In the pancreas, strong reactivity was confined to the exocrine tissue (Fig. 2 D, bottom right). These mice also contained high levels of IgG antinuclear auto-Abs (ANAs) in their sera (Fig. 2 E). These findings show that the organs affected by a lymphoid infiltrate are also the targets of organ-specific auto-Abs.

The splenomegaly in WT mice reconstituted with *Nfκb1*$^{-/-}$ BM was primarily attributed to an elevated number of mature B cells (Fig. 3 A). The altered distribution of peripheral B cell subsets resembled that seen in aged *Nfκb1*$^{-/-}$ mice, with a prominent increase in the numbers of Fo B cells, GC B cells, and T_{FH} cells (Fig. 3, B–D; and Fig. S2, A–C). We also detected an expanded population of host-derived CD4^{+} T cells that contributed to the pool of T_{FH} cells (not depicted). Examination of the *Nfκb1*$^{-/-}$ Fo B cells revealed heat-stable antigen expression was reduced (HSA^{lo}) and activation markers were acquired (CD80, CD86, CD40, and MHC II; Fig. 3 G). In marked contrast to our findings in *Nfκb1*$^{-/-}$ mice, the GC B cells in NFκB1 chimeras expressed normal levels of cell surface FAS and GL-7 and formed bona fide GCs in the spleen that were significantly larger than the GCs observed in the control chimeras (Fig. 3, E and F; and Fig. S2 B). Collectively, our results demonstrate that NFκB1 serves an essential role in the hematopoietic compartment to limit aberrant lymphoproliferation and prevent the development of multiorgan autoimmune disease.

Disease development is caused by the loss of NFκB1 function and not impaired ERK signaling

To determine whether the inflammation in aging *Nfκb1*$^{-/-}$ mice and in WT mice reconstituted with *Nfκb1*$^{-/-}$ BM was the result of impaired Tpl-2–regulated ERK activity or the loss of p50-dependent gene expression, irradiated ly5.1^{+} WT mice were reconstituted with *Map3k8*$^{-/-}$ BM. At the time when disease was observed in WT mice transplanted with *Nfκb1*$^{-/-}$ BM, we found no evidence of lymphoproliferative or autoimmune disease in chimeras with a Tpl-2–deficient hematopoietic system (Fig. 3, G–I). Therefore, the development of lymphoproliferative and multiorgan autoimmune disease in aging *Nfκb1*$^{-/-}$ mice and WT hosts reconstituted with *Nfκb1*$^{-/-}$ BM is the result of the loss of p105/p50, not impaired ERK activity.

immunofluorescence staining with anti-B220 (B cells; green) and PNA lectin (GC cells; red). Images show individual and composite stains. Arrows indicate bona fide GCs; an atypical GC area (square bracket) is shown in the *Nfκb1*$^{-/-}$ spleen (>12 mo = 455 ± 68 d). (G) Absolute numbers of T_{FH} cells (CD4^{+}PD-1^{+} CXCR5^{+}). Data in C–G are representative of at least two independent experiments (n = 3–5 mice/genotype). All graphs are shown as the mean ± SEM, and statistical significance was determined using unpaired Student's t tests. *, $P \leq 0.05$, **, $P < 0.001$. ns, not significant. Bars, 100 µm.

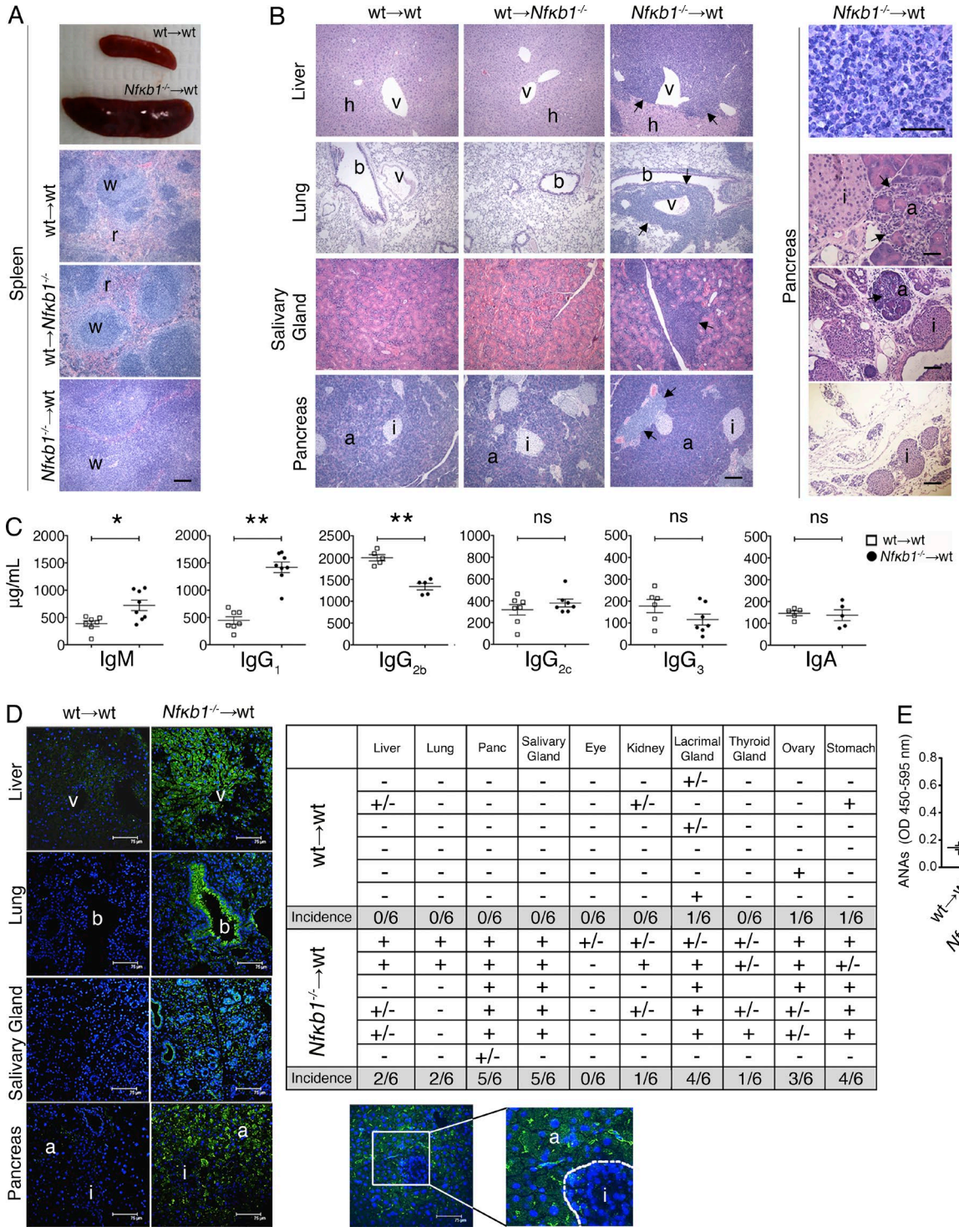

	Liver	Lung	Panc	Salivary Gland	Eye	Kidney	Lacrimal Gland	Thyroid Gland	Ovary	Stomach
wt→wt	-	-	-	-	-	-	+/-	-	-	-
	+/-	-	-	-	-	+/-	-	-	-	+
	-	-	-	-	-	-	+/-	-	-	-
	-	-	-	-	-	-	-	-	-	-
	-	-	-	-	-	-	-	-	+	-
	-	-	-	-	-	-	+	-	-	-
Incidence	0/6	0/6	0/6	0/6	0/6	0/6	1/6	0/6	1/6	1/6
Nfκb1-/-→wt	+	+	+	+	+/-	+/-	+/-	+/-	+	+
	+	+	+	+	-	+	+	+/-	+	+/-
	-	-	+	+	-	-	+		+	+
	+/-	-	+	+	-	+/-	+	+/-	+/-	+
	+/-	-	+	+	-	-	+	+	+/-	+
	-	-	+/-	-	-	-	-	-	-	-
Incidence	2/6	2/6	5/6	5/6	0/6	1/6	4/6	1/6	3/6	4/6

Figure 2. **Selective loss of NFκB1 in hematopoietic cells causes multiorgan autoimmunity.** (A–E) Lethally irradiated ly5.1+ WT and *Nfκb1*$^{-/-}$ (ly5.2+) hosts were reconstituted with *Nfκb1*$^{-/-}$ (ly5.2+) or ly5.1+ WT BM cells, respectively. As controls, ly5.1+ WT hosts were reconstituted with WT (ly5.2+) BM. Chimeras were analyzed 7 mo after engraftment. (A) Splenomegaly in hosts reconstituted with *Nfκb1*$^{-/-}$ BM; w, white pulp; r, red pulp. (B) Left: H&E-stained tissue sections (bars = 200 µm). Top right: Mononuclear cell infiltrate in the pancreas (scale = 50 µm). Bottom right: Cell infiltrate (arrow) and acinar cell destruction in the pancreas (top-to-bottom bars = 50, 100 and 200 µm); v, venule; h, hepatocyte; b, bronci; a, acinar cells; i, islet. (C–E) Screening of sera from BM-reconstituted mice. (C) Serum Ig titers (mean ± SEM); each symbol represents one mouse. (D) Left: Detection of auto-Abs by indirect immunofluorescence as described in Fig. 1 B; green: positive staining, blue: DAPI nuclear counterstain. Images are representative of six mice per group. Top right: Summary of auto-Abs to specified organs:

NFκB1-deficient Fo B cells display increased inflammatory and autoimmune transcripts

To determine the mechanisms underlying the increased activation of *Nfκb1*$^{-/-}$ Fo B cells, mRNA expression profiling was performed on Fo B cells from young WT and *Nfκb1*$^{-/-}$ mice. Of the 84 genes examined that were associated with inflammation and autoimmunity, 21 were differentially expressed (>1.5-fold) in *Nfκb1*$^{-/-}$ Fo B cells compared with WT counterparts (Fig. 4 A). Prominent changes in mRNA expression were detected for *C4b* (4.6-fold increase), *Cxcl9* (4.18-fold increase), *Ptgs2* (3.87-fold decrease), *Bcl-6* (2.6-fold increase), and *Il-6* (3.36-fold increase). Importantly, this indicates that the Fo B cells have a pattern of gene expression that is consistent with the defects seen in the *Nfκb1*$^{-/-}$ mice.

Deregulated production of IL-6 is driven by the loss of NFκB1 in Fo B cells

Aging *Nfκb1*$^{-/-}$ mice contain elevated serum levels of proinflammatory cytokines, including TNF and IL-6 (Jurk et al., 2014). Interestingly, an increase in the serum levels of IL-6, but not IL-1α or TNF, coincided with disease onset at 4 mo in *Nfκb1*$^{-/-}$ BM chimeras, whereas both IL-1 and IL-6 were significantly elevated at the later stage of disease pathogenesis (Fig. 4 B).

To determine whether high *Il-6* transcript levels of *Nfκb1*$^{-/-}$ Fo B cells coincide with elevated IL-6 production by these cells, splenic sections from aged BM-reconstituted mice were subjected to immunofluorescence staining with anti–IL-6 Abs. Although low levels of IL-6 staining were seen in control spleens, extensive staining was detected in the spleens of *Nfκb1*$^{-/-}$ BM chimeras (Fig. 4 C). Two-color staining using anti–IL-6 and anti-B220 Abs revealed that IL-6 expression was confined to the B cell follicles within a subpopulation of B cells that resided in close proximity to GC B cells (Fig. 4 C). IL-6 was also observed in the spleens of *Nfκb1*$^{-/-}$ mice, with strong focal staining detected in the aging *Nfκb1*$^{-/-}$ mice (Fig. 5 A). Almost all IL-6 staining colocalized with IgM but not with IgG_1 or IgD (Fig. 5 A). Prominent staining for CD80 and CD86 was only observed in the aged *Nfκb1*$^{-/-}$ mice (Fig. 5 A), but this did not colocalize with the majority of IL-6–expressing cells, which were primarily positive for Ki67 in both young and aging *Nfκb1*$^{-/-}$ mice (Fig. 5 A). These results suggest that a population of peripheral IgM^{+}Ki67^{+}*Nfκb1*$^{-/-}$ B cells secrete abnormally high amounts of IL-6, a conclusion confirmed by the increased numbers of IL-6–producing *Nfκb1*$^{-/-}$ B cells detected by intracellular staining and flow cytometric analysis (Fig. 5 B).

Despite these findings, it was unclear whether excessive IL-6 production by *Nfκb1*$^{-/-}$ B cells was an indirect consequence of the inflammatory milieu. We addressed this by examining naive Fo B cells in 6-wk-old *Nfκb1*$^{-/-}$ mice before disease. When cultured without stimuli, *Nfκb1*$^{-/-}$ Fo B cells produced significantly more IL-6 than their WT counterparts (Fig. 5 C). Collectively, these findings suggest that the excessive IL-6 production is linked to an absence of NFκB1 in B cells and that IL-6 is a major mediator of chronic disease in *Nfκb1*$^{-/-}$ mice.

Spontaneous GC formation and enhanced IL-6 production is caused by the loss of NFκB1 in B cells

To address whether the altered function of Fo B cells was the result of an intrinsic loss of NFκB1, mixed BM (mBM) chimeric mice were established by engrafting lethally irradiated ly5.1^{+} WT hosts with an equal mix (1:1) of ly5.1^{+} WT and ly5.2^{+} *Nfκb1*$^{-/-}$ BM or control (WT; ly5.1^{+} and ly5.2^{+}) BM. When exposed to the same hematopoietic environment, only *Nfκb1*$^{-/-}$ Fo B cells displayed an activated phenotype (CD80^{hi}CD86^{hi}CD40^{hi}) and increased cell division (Fig. 6, A and B; and not depicted). Bcl-6, which serves as a master transcriptional regulator of GC B cells (Basso and Dalla-Favera, 2012), although expressed at low levels in WT and *Nfκb1*$^{-/-}$ transitional B cells, was elevated in *Nfκb1*$^{-/-}$ Fo B cells (Fig. 6 C), suggesting that these cells are committed to GC B cell differentiation. Consistent with this notion, the *Nfκb1*$^{-/-}$ but not WT GC B cell population was expanded, and the number of IgG_1^{+} *Nfκb1*$^{-/-}$ B cells significantly increased (Fig. 6, A and B). Bcl-6 expression was elevated in *Nfκb1*$^{-/-}$ Fo but not GC B cells, with intracellular IL-6 staining confirming that only *Nfκb1*$^{-/-}$ Fo B cells produce excessive amounts of IL-6 (Fig. 6, D and F). Together, these data indicate that NFκB1 plays an essential intrinsic role in mature Fo B cells to prevent the uncontrolled production of IL-6 and the spontaneous generation of GC B cells.

To determine the contribution of CD4^{+} T cells to *Nfκb1*$^{-/-}$ GC B cell differentiation, WT and *Nfκb1*$^{-/-}$ T_{FH} cells were examined in mBM-reconstituted mice. Although a small population of mature T_{FH} cells was detected in control mBM chimeras, a threefold increase in T_{FH} cells of both genotypes was observed in mutant mBM chimeras (Fig. 6 E). This indicates that cell-extrinsic signals promote enhanced T_{FH} cell differentiation in *Nfκb1*$^{-/-}$ mice.

positive (+), negative (–), and trace staining (+/–). Bottom right: Enlarged image of the pancreas from the left side shows auto-Ab reactivity primarily against the exocrine but not endocrine tissue. Dashed line delineates the border between the acinar and islet cells. Bars, 75 µm. (E) Serum ANA levels (mean ± SEM) measured by ELISA. Each symbol represents one mouse. Statistical significance in C and E was determined by independent samples Student's *t* tests. *, $P < 0.05$; **, $P < 0.001$. ns, not significant. In A and B, results are representative of $n = 7$ (WT→WT and *Nfκb1*$^{-/-}$→WT) or $n = 3$ (WT→*Nfκb1*$^{-/-}$) mice. Data in A–E are derived from more than two independent experiments.

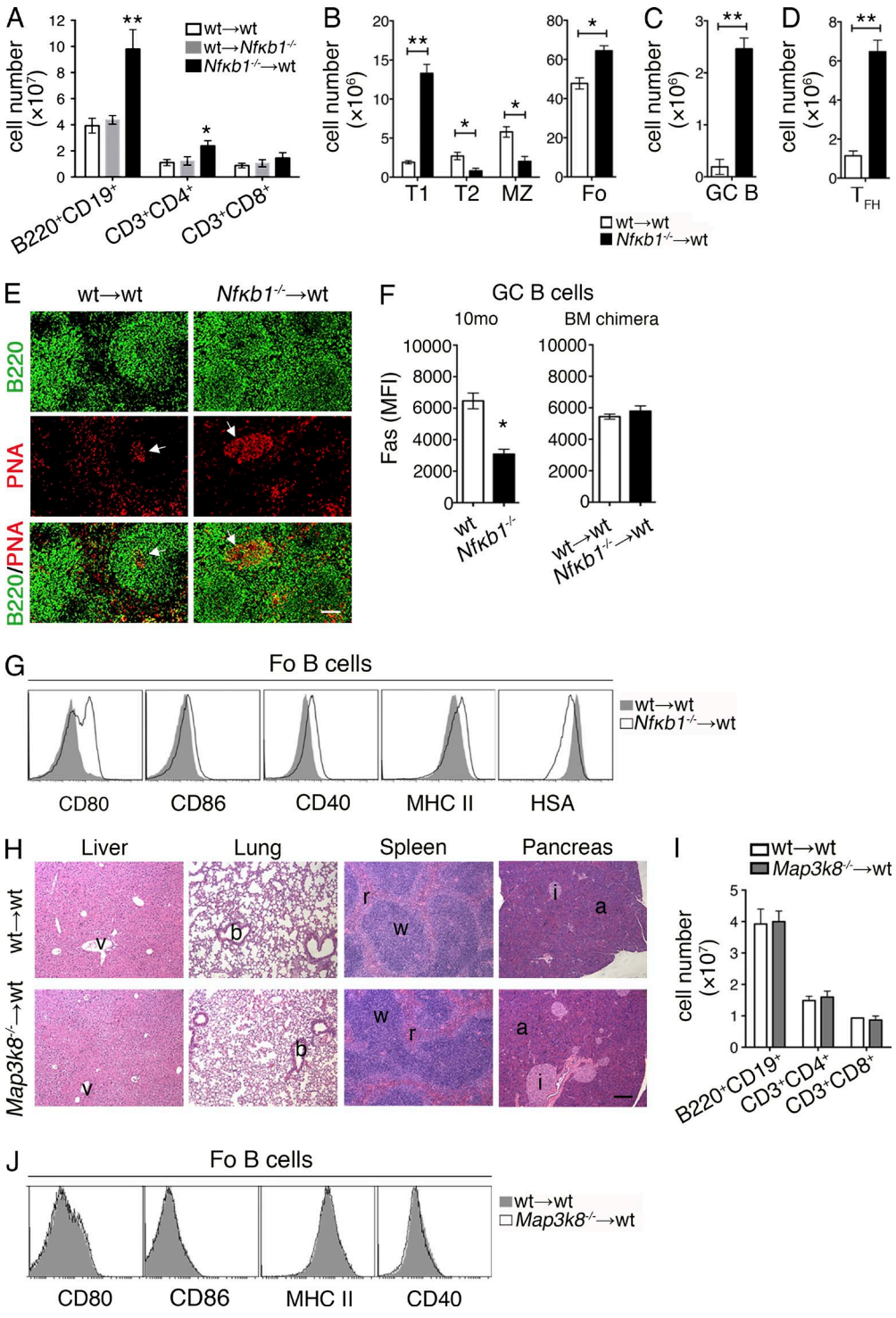

Figure 3. **Absence of NFκB1 in hematopoietic cells alters peripheral B cell homeostasis.** BM chimera mice were established as described in Fig 2. Spleens were harvested from control (WT→WT) and mutant (WT→*Nfκb1*$^{-/-}$, *Nfκb1*$^{-/-}$→WT, and *Map3k8*$^{-/-}$→WT) BM-reconstituted mice 7–10 mo after transplantation. (A–D) Flow cytometric analysis of T and B cell subsets in the spleens of BM chimeric mice. (A) Lymphoid cell numbers (three to seven mice per group from two independent experiments). (B) Absolute numbers of B cell subsets (see gating strategy in Fig. S2). (C and D) GC B (B220^{+}FAS^{+}GL7^{+}; C) and T_{FH} (CD4^{+}CXCR5^{+}ICOS^{+}PD-1^{+}; D) cell numbers. (E) Spleen cryosections stained with anti-B220 (B cells; green) and PNA lectin (GC; red). Arrows indicate GC areas. (F) FAS expression (mean fluorescence intensity [MFI]) examined by flow cytometry on GC B cells from 10-mo-old mice or BM chimera mice. (G) Cell surface markers examined by flow cytometry on Fo B cells. Results from B–G are derived from at least three independent experiments (n = 6 mice/group).

In vivo neutralization of IL-6 reduces GC B and T_{FH} cell differentiation

Our findings were consistent with a model whereby IL-6–secreting *Nfκb1*$^{-/-}$ Fo B cells facilitate increased T_{FH} cell differentiation. To test this hypothesis, mBM chimeric mice were treated with neutralizing anti–IL-6 Abs or control Ig isotype–matched Abs. After 6 wk of biweekly injections, only mBM chimeric mice injected with anti–IL-6 Abs displayed several notable changes in both the B and T cell compartment (Fig. 7). The distribution of *Nfκb1*$^{-/-}$ transitional and MZ B cells was not affected by IL-6 neutralization, but *Nfκb1*$^{-/-}$ Fo and GC B cell numbers were significantly reduced (Fig. 7, A–C; and Fig. S3 A), in particular the number of proliferating *Nfκb1*$^{-/-}$ Fo B cells (Fig. 7 B). Both WT and *Nfκb1*$^{-/-}$ T_{FH} cell numbers were also reduced to near-normal levels by anti–IL-6 Ab treatment (Figs. 7 D and S3 A), and tissue-specific serum auto-Ab levels were lower (Fig. 7, G and H). These results demonstrate that deregulated IL-6 production is responsible for the abnormal increase in Fo B cells and the excessive differentiation of GC B and T_{FH} cells in mice lacking NFκB1.

IL-6 can signal via the classical pathway or by engaging a trans-signaling pathway where soluble IL-6/IL-6R complexes associate with gp130 on target cells (Rose-John, 2012). To determine which pathway IL-6 uses to drive the B cell abnormalities in *Nfκb1*$^{-/-}$ mice, mBM chimeras were treated with a soluble form of gp130 (sgp130Fc) that only inhibits IL-6 trans-signaling (Schuett et al., 2012). In marked contrast to the application of anti–IL-6 Abs, which block both IL-6 signaling pathways, treatment with sgp130Fc did not inhibit the excessive differentiation of T_{FH} or GC B cells caused by the absence of NFκB1 (Fig. 7, E and F; and Fig. S3 B). In fact, WT T_{FH} cell differentiation was significantly enhanced, which could reflect the change in IL-6 levels that regulate the balance of specific T cell subsets (Rose-John, 2012). These findings establish that classical IL-6 signaling promotes Fo B cell accumulation and enhanced GC B and T_{FH} cell differentiation in *Nfκb1*$^{-/-}$ mice.

Absence of NFκB1 mediates the aberrant activation of Fo B cells

To determine how the increased secretion of IL-6 affects the function of *Nfκb1*$^{-/-}$ Fo B cells, WT and *Nfκb1*$^{-/-}$ Fo B cells were isolated from young mice and stimulated with graded concentrations of antigen receptor agonists. As a measure of early activation, we examined calcium mobilization. After BCR cross-linking, early B cell signaling was found to be enhanced in *Nfκb1*$^{-/-}$ Fo B cells, with a sharp increase in intracellular calcium flux $[Ca^{2+}]_i$ (Fig. 8, A and B). Differences in $[Ca^{2+}]_i$ levels between WT and *Nfκb1*$^{-/-}$ Fo B cells were greatest at suboptimal concentrations (2, 5, and 10 µg/ml) of anti–IgM $F(ab')_2$ Ab fragments, with $[Ca^{2+}]_i$ levels in WT Fo B cells being undetectable (2 µg/ml) or low (5 and 10 µg/ml). At optimal concentrations (20 µg/ml) of anti–IgM $F(ab')_2$ Ab fragments, $[Ca^{2+}]_i$ levels were comparable between WT and *Nfκb1*$^{-/-}$ Fo B cells. Interestingly, enhanced $[Ca^{2+}]_i$ levels were primarily associated with IgM^{hi} *Nfκb1*$^{-/-}$ Fo B cells, which includes the IL-6–secreting *Nfκb1*$^{-/-}$ B cells, whereas IgM^{lo}*Nfκb1*$^{-/-}$ Fo B cells responded like their WT counterparts (Fig. 8 B).

To establish whether IL-6 exposure alone is sufficient for the increased antigen responsiveness of IgM^{hi} *Nfκb1*$^{-/-}$ Fo B cells, we examined ly5.1^{+} WT and *Nfκb1*$^{-/-}$ splenic B cells from mBM-reconstituted mice using low concentrations of anti–IgM $F(ab')_2$ (Fig. 8 C). The $[Ca^{2+}]_i$ levels were significantly higher in the *Nfκb1*$^{-/-}$ but not WT Fo B cells (Fig. 8 C), which resembled our findings in *Nfκb1*$^{-/-}$ mice. Therefore, exposure to increased IL-6 levels in vivo is insufficient for enhancing the stimulatory response of WT B cells. Instead, our findings suggest that autocrine IL-6 signaling allows *Nfκb1*$^{-/-}$ Fo B cells to be activated by low levels of BCR stimulation.

Next, proliferation was assessed using CFSE-stained WT and *Nfκb1*$^{-/-}$ Fo B cells. No proliferation of Fo B cells of either genotype was detected in the absence of BCR ligation (Fig. 8 D). However, the proliferation of *Nfκb1*$^{-/-}$ Fo B cells was markedly higher in response to BCR cross-linking with suboptimal concentrations of anti–IgM $F(ab')_2$ applied alone or combined with CD40 stimulation or in response to suboptimal concentrations of CpG (Fig. 8, D and E). In contrast, WT and *Nfκb1*$^{-/-}$ Fo B cell proliferation was comparable at optimal concentrations of these B cell agonists. Overall, WT and *Nfκb1*$^{-/-}$ Fo B cells showed similar proliferation kinetics, but a greater proportion of proliferating *Nfκb1*$^{-/-}$ Fo B cells was detected at suboptimal mitogen concentrations. Our findings indicate that NFκB1 prevents Fo B cells from responding to low levels of signaling through the BCR or TLR9.

Increased autocrine IL-6/IL-6R signaling enhances the proliferation of *Nfκb1*$^{-/-}$ Fo B cells

To determine whether the enhanced sensitivity of *Nfκb1*$^{-/-}$ Fo B cells to stimulation was the result of autocrine or paracrine IL-6/IL-6R signaling, co-cultures of WT and *Nfκb1*$^{-/-}$ Fo B cells were subjected to BCR cross-linking in the presence of neutralizing anti–IL-6 or Ig isotype–matched control Abs. The control Ab did not affect the calcium mobilization or proliferation of *Nfκb1*$^{-/-}$ Fo B cells, but blocking IL-6 reduced the $[Ca^{2+}]_i$ response and restored proliferation and cell numbers to normal levels (Fig. 9, A–D; and Fig. S4). IL-6 neutralization had no impact on the $[Ca^{2+}]_i$ levels or proliferation of WT Fo B cells (Fig. 9, A–D). Under similar conditions, the addition of exogenous IL-6 to B cell cultures

(H) H&E-stained tissue sections from control and Tpl-2–deficient chimera mice. (I) Absolute cell numbers of splenic lymphoid cells. (J) Flow cytometric analysis of Fo B cells. In H–J, results are from two independent experiments; four to five mice per group. Graphs are shown as the mean ± SEM, and statistical significance was determined using unpaired Student's *t* tests. *, $P < 0.05$; **, $P < 0.001$. Bars: (E) 50 µm; (H) 200 µm.

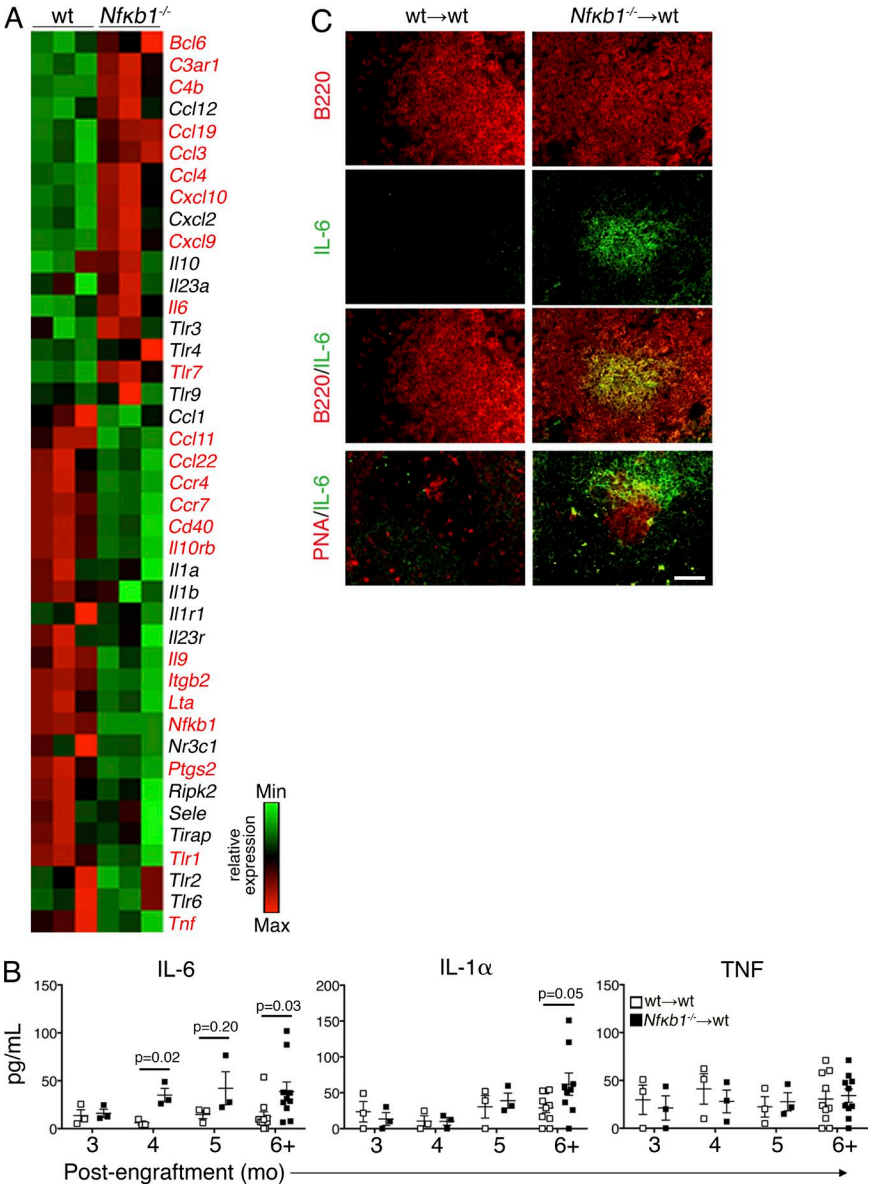

Figure 4. **Loss of NFκB1 in B cells is linked with deregulated IL-6 production.** (A) Relative mRNA expression of 84 genes associated with inflammation and autoimmunity was analyzed in Fo B cells from the LNs of 6–8-wk-old WT and *Nfκb1*$^{-/-}$ mice. Genes in red denote statistical significance ($P < 0.05$). Data are derived from three independent experiments, each with pooled samples from four mice per genotype ($n = 12$). (B) Serum cytokine levels in BM-reconstituted mice at the indicated time points (each symbol represents one mouse; two or three independent experiments). P-values as indicated were determined by unpaired Student's *t* test. (C) Spleen cryosections were stained with anti-B220 (B cells; red) or PNA lectin (GG; red) combined with anti–IL-6 (green). Colocalization is shown in yellow ($n = 4$ mice/group; three independent experiments). Bar, 50 µm.

revealed that WT Fo B cells now displayed enhanced calcium mobilization, proliferation, and increased cell numbers that resembled *Nfκb1*$^{-/-}$ Fo B cells (Fig. 9, A–D). This demonstrates that paracrine IL-6 signaling is sufficient to increase the activation and proliferation of both WT and *Nfκb1*$^{-/-}$ Fo B cells, whereas autocrine IL-6/IL-6R signaling drives the enhanced activation and proliferation of *Nfκb1*$^{-/-}$ Fo B cells.

p50-NFκB1 is a direct negative regulator of IL-6 gene expression in Fo B cells

The aberrant production of IL-6 by *Nfκb1*$^{-/-}$ Fo B cells raised the question of whether p50-NFκB1 directly regulates the *Il-6* gene in Fo B cells. Using imaging flow cytometry, we examined the intracellular localization of p50-NFκB1 and its major dimer partner, RELA (Fig. 10 A). p50-NFκB1 was almost exclusively in the nuclei of WT Fo B cells, whereas the majority of RELA was cytoplasmic (Fig. 10, A and B). In contrast, there was significant colocalization of RELA with the nuclear dye in *Nfκb1*$^{-/-}$ Fo B cells (Fig. 10, A and B), indicating that the absence of p50-NFκB1 increases RELA nuclear localization.

Using the TRANSFAC database, four consensus κB-binding sites predicted to bind p50-NFκB1 with high probability were identified in the *Il-6* locus (Fig. 10 C). Chromatin immunoprecipitation (ChIP) was used to validate these putative p50-NFκB1–binding sites. In WT Fo B cells, p50-NFκB1 bound to all four sites, whereas no or only minimal RELA binding was detected (Fig. 10 D). Interestingly, with the exception of region 2, RELA binding to each κB site was significantly higher in *Nfκb1*$^{-/-}$ Fo B cells (Fig. 10 D). These

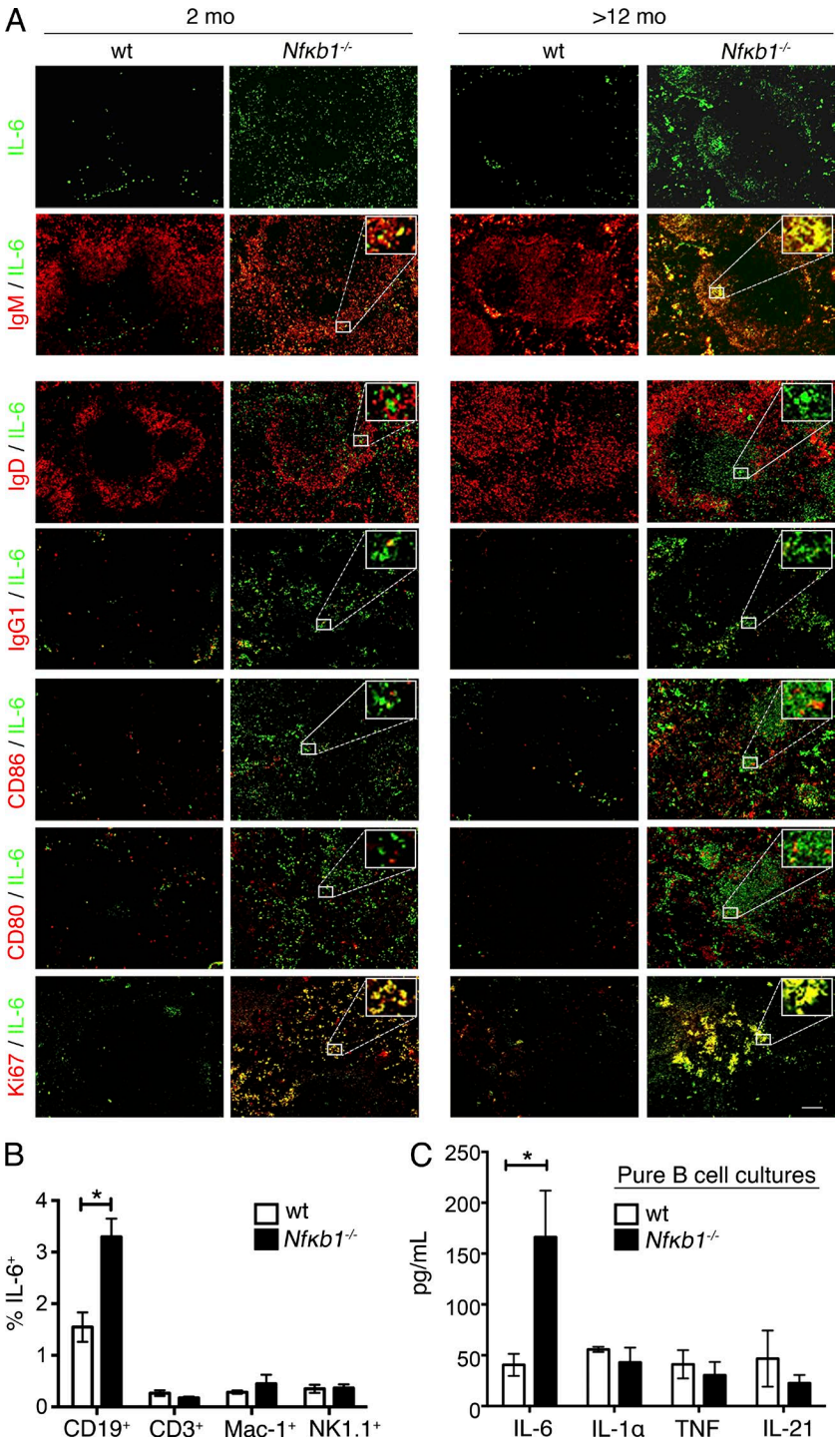

Figure 5. **Increased IL-6 production by a population of IgM$^+$Ki67$^+$*Nfκb1*$^{-/-}$ Fo B cells.** (A) Splenic cryosections from WT and *Nfκb1*$^{-/-}$ mice were subjected to single anti–IL-6 Ab staining (green) and in combination with a panel of Abs (red). Colocalization (yellow) was detected by merging the images and shown (inset) for a representative area. (B and C) Cytokine analysis in the spleens of young WT and *Nfκb1*$^{-/-}$ mice. (B) Percentage of IL-6–producing cells as determined by intracellular staining and flow cytometric analysis. (C) Secreted cytokines measured by a cytokine bead array in the supernatant of Fo B cell cultures at 72 h. Data are presented as the mean ± SEM. In A–C, $n \geq 3$ mice/genotype (tested in two to four independent experiments). Statistical significance was determined using independent samples Student's *t* tests. *, $P < 0.05$. Bar, 100 µm.

results demonstrate that the negative regulation of *Il-6* by p50-NFκB1 in Fo B cells coincides with RELA being excluded from binding these κB elements in the *Il-6* locus.

DISCUSSION

Herein, we identify a novel role for NFκB1 in preventing the development of lymphoproliferative and multiorgan autoimmune disease.The absence of NFκB1 promotes the aberrant expansion of Fo B cells that leads to enhanced T_{FH} and GC B cell differentiation. In aged NFκB1-deficient mice, this culminates in autoimmune pathology that includes hyper–γ-globulinemia, tissue-specific auto-Abs, and multiorgan immune cell infiltrates. Disease pathology was largely attributed to the excessive production of IL-6 by a population of IgM$^+$Ki67$^+$ *Nfκb1*$^{-/-}$

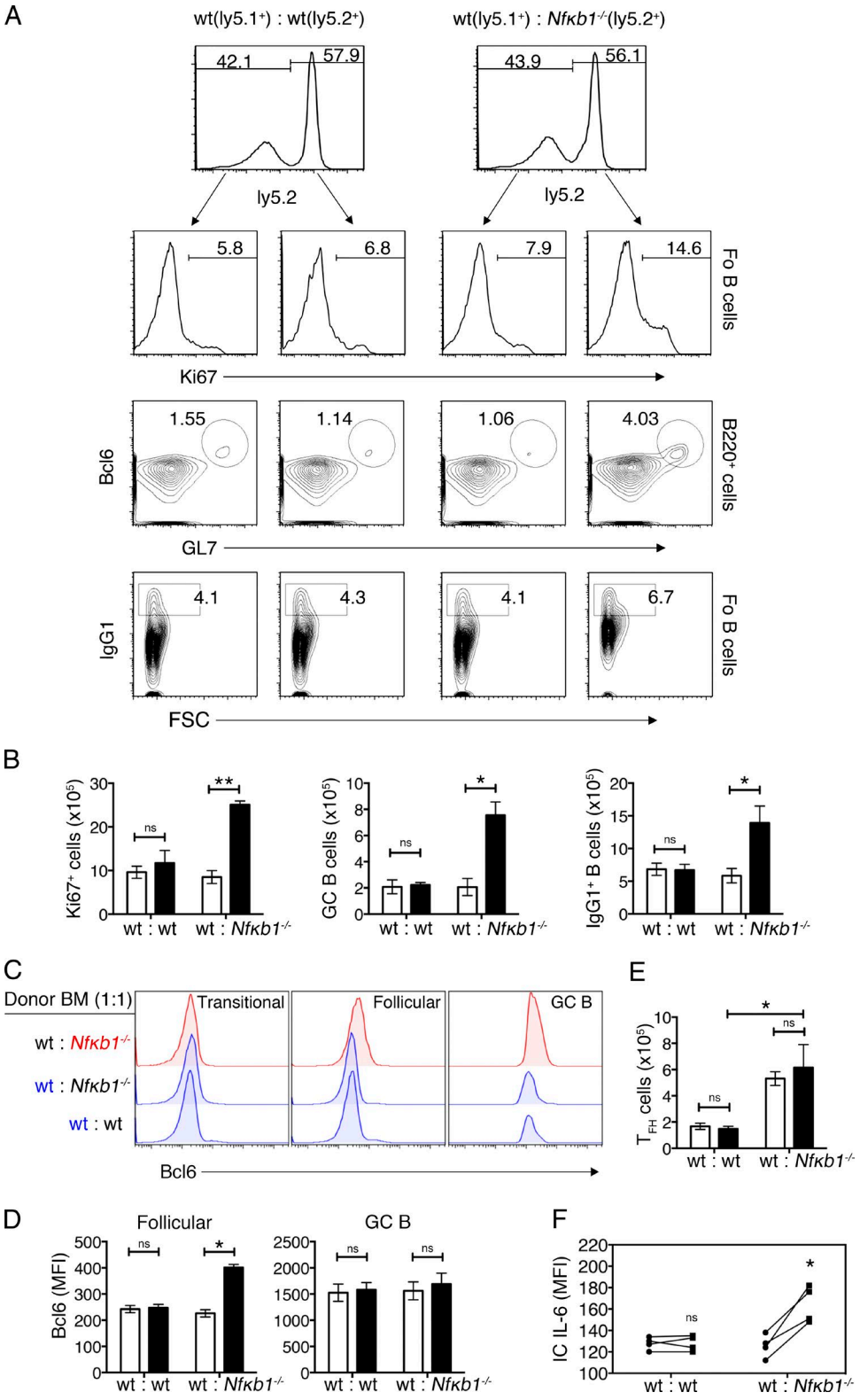

Figure 6. **Enhanced B cell differentiation is the result of the cell-intrinsic loss of NFκB1.** (A–F) mBM chimera mice were generated by mixing ly5.1+ WT BM cells with *Nfκb1*$^{-/-}$ or WT (both ly5.2+) BM cells (1:1 ratio) and transferred into lethally irradiated ly5.1+ WT hosts. After 16 wk, spleens were isolated and processed for flow cytometry analysis. Splenocytes were defined on the basis of ly5.2 expression. (A) Ki67 expression in Fo B cells (B220+CD21^{int}IgM^{lo}); dot plots show GL7 versus Bcl6 staining gated on B220+ cells (GCs; GL7+Bcl6+) and IgG1 staining versus FSC gated on Fo B cells (IgG1+ B cells). The numbers

Fo B cells, with IL-6 acting in an autocrine/paracrine manner to alter the function and homeostasis of *Nfκb1*$^{-/-}$ Fo B cells and promote the excessive differentiation of *Nfκb1*$^{-/-}$ T_{FH} and GC B cells. Our findings show that NFκB1 is a negative regulator of *Il-6* transcription in Fo B cells that prevents RELA-dependent *Il-6* transcription. Collectively, this establishes that NFκB1 maintains the homeostasis of mature Fo B cells and prevents the development of autoimmune disease, in part by suppressing *Il-6* transcription.

Consistent with other studies (Oakley et al., 2005; Bernal et al., 2014; Jurk et al., 2014), we show that *Nfκb1*$^{-/-}$ mice develop a chronic inflammatory condition. Our observations indicate that the premature death of *Nfκb1*$^{-/-}$ mice is associated with the development of multiorgan autoimmune disease involving auto-Abs targeting various tissues. Using BM-reconstituted mice, we established that the absence of NFκB1 within hematopoietic cells was sufficient to induce autoimmune disease. The abnormalities observed in the *Nfκb1*$^{-/-}$ chimeras resembled those seen in the aged *Nfκb1*$^{-/-}$ mice, but glomerulonephritis and gastrointestinal pathology were not seen in BM-reconstituted mice. The inability of *Nfκb1*$^{-/-}$ hematopoietic cells to recapitulate all aspects of disease seen in *Nfκb1*$^{-/-}$ mice indicates that a loss of NFκB1 in nonhematopoietic cells is necessary but insufficient to induce certain pathologies. This interpretation is consistent with the role for NFκB1 in regulating inflammatory cytokine production by gastric and intestinal epithelial cells (Erdman et al., 2001; Burkitt et al., 2013).

Autoimmune pathology in aged NFκB1-deficient mice was accompanied by progressive changes in the peripheral B cell compartment. Aging *Nfκb1*$^{-/-}$ mice accumulate a population of IL-6–secreting Fo B cells that promote autoimmune disease, splenomegaly, and lymphoid infiltrates in various organs. It remains unclear how this population of IL-6–producing B cells arises in the periphery of young *Nfκb1*$^{-/-}$ mice. With roles ascribed to NFκB1 in transitional B cell survival (Snapper et al., 1996) and the consequent impaired transition of *Nfκb1*$^{-/-}$ B cells from the T1 to T2 stage, this could lead to a breakdown of B cell tolerance, resulting in the generation of mature B cells with an autoreactive-biased BCR repertoire. In the aging and BM chimeric *Nfκb1*$^{-/-}$ mice, disease also tracks with a population of activated splenic Fo B cells with the vast majority of IL-6–secreting *Nfκb1*$^{-/-}$ B cells residing in close proximity. Although it remains unclear how the activated B cells contribute to the disease phenotype of the *Nfκb1*$^{-/-}$ mice, our evidence suggests that increased IL-6 levels promote the generation of activated *Nfκb1*$^{-/-}$ B cells, which contributes to enhanced GC B cell differentiation. In mBM-reconstituted mice, only the NFκB1-deficient B cell compartment contributed to the expanded population of Fo B cells, which is consistent with a critical B cell–intrinsic role for NFκB1 (Sha et al., 1995; Snapper et al., 1996). The finding that Bcl-6 expression is abnormally elevated suggests that *Nfκb1*$^{-/-}$ Fo B cells have a propensity to become activated and form GC B cells. This coincides with *Nfκb1*$^{-/-}$ Fo B cells alone contributing to the increased GC B cells numbers in the mBM chimeric mice. Collectively, this shows that an absence of NFκB1 has a significant cell-intrinsic impact on the Fo B cell population.

Although NFκB activity is very low or undetectable in most human GC B cells, a subset of centrocytes expresses nuclear RELA, c-REL, and p50-NFκB1 (Basso et al., 2004; Victora et al., 2010). In the absence of NFκB1, GC B cells expressed reduced levels of cell surface FAS and GL-7, with transient GC formation severely disrupted in both young and aged *Nfκb1*$^{-/-}$ mice. This failure to form bona fide GC structures in the *Nfκb1*$^{-/-}$ mice is likely to account for the significantly reduced serum IgG_1 levels. A clue to understanding these findings came from the BM chimera models, where the expansion of host-derived T cells in the complete BM chimeras or of WT T cells in the mBM chimeras resulted in the accumulation of *Nfκb1*$^{-/-}$ GC B cells with a normal phenotype and the formation of bona fide GC structures. Although excessive numbers of T_{FH} cells are intimately associated with *Nfκb1*$^{-/-}$ GC B cell differentiation, the presence of WT T_{FH} cells in the *Nfκb1*$^{-/-}$ BM-reconstituted mice coincided with the increased levels of serum IgG_1 and ANAs. We propose that WT T_{FH} cells accelerate disease development in the BM chimeric mice by facilitating Fo B cell differentiation and GC formation. Overall, these results implicate T_{FH} cells in the spontaneous formation of GC B cells and the autoimmune phenotype observed in aging *Nfκb1*$^{-/-}$ mice. These data also raise doubts about the functional competency of T_{FH} cells in *Nfκb1*$^{-/-}$ mice.

We have previously shown that the *Nfκb1*$^{-/-}$ mice immunized with NP-KLH displayed a markedly reduced anti–NP-KLH (IgG_1) response (Pohl et al., 2002). The size and frequency of GCs was significantly reduced in the spleens, but clearly demarcated GCs were formed in the absence of NFκB1. Similarly, the IgG_1 response was diminished in immunized *c-rel*$^{-/-}$ mice, with small irregular GCs detected. However, immunized *Nfκb1*$^{-/-}$*c-rel*$^{-/-}$ mice were completely devoid of GCs, indicating that both c-REL and NFκB1 play critical nonredundant roles in GC formation in response to T cell–dependent antigens. Studying the role of NFκB1 in GC B cells is currently restricted by the absence of a conditionally

represent percentages. (B) Absolute cell numbers of Ki67$^+$ Fo B cells, GC B cells, and IgG1$^+$ B cells. (C) Expression of Bcl-6 in B cell subsets derived from WT or *Nfκb1*$^{-/-}$ BM cells in mBM chimeric mice. (D) Bcl-6 expression (mean fluorescence intensity [MFI]) in Fo and GC B cells. (E) Absolute numbers of WT and *Nfκb1*$^{-/-}$ T_{FH} cells (CD4$^+$CXCR5$^+$PD-1$^+$). (F) Intracellular IL-6 expression in Fo B cells from mBM chimera mice. Results were derived from two independent cohorts of reconstituted mice (n = 6/group). Statistical significance was determined using independent or paired samples Student's t tests as appropriate. *, $P < 0.05$; **, $P < 0.001$. ns, not significant.

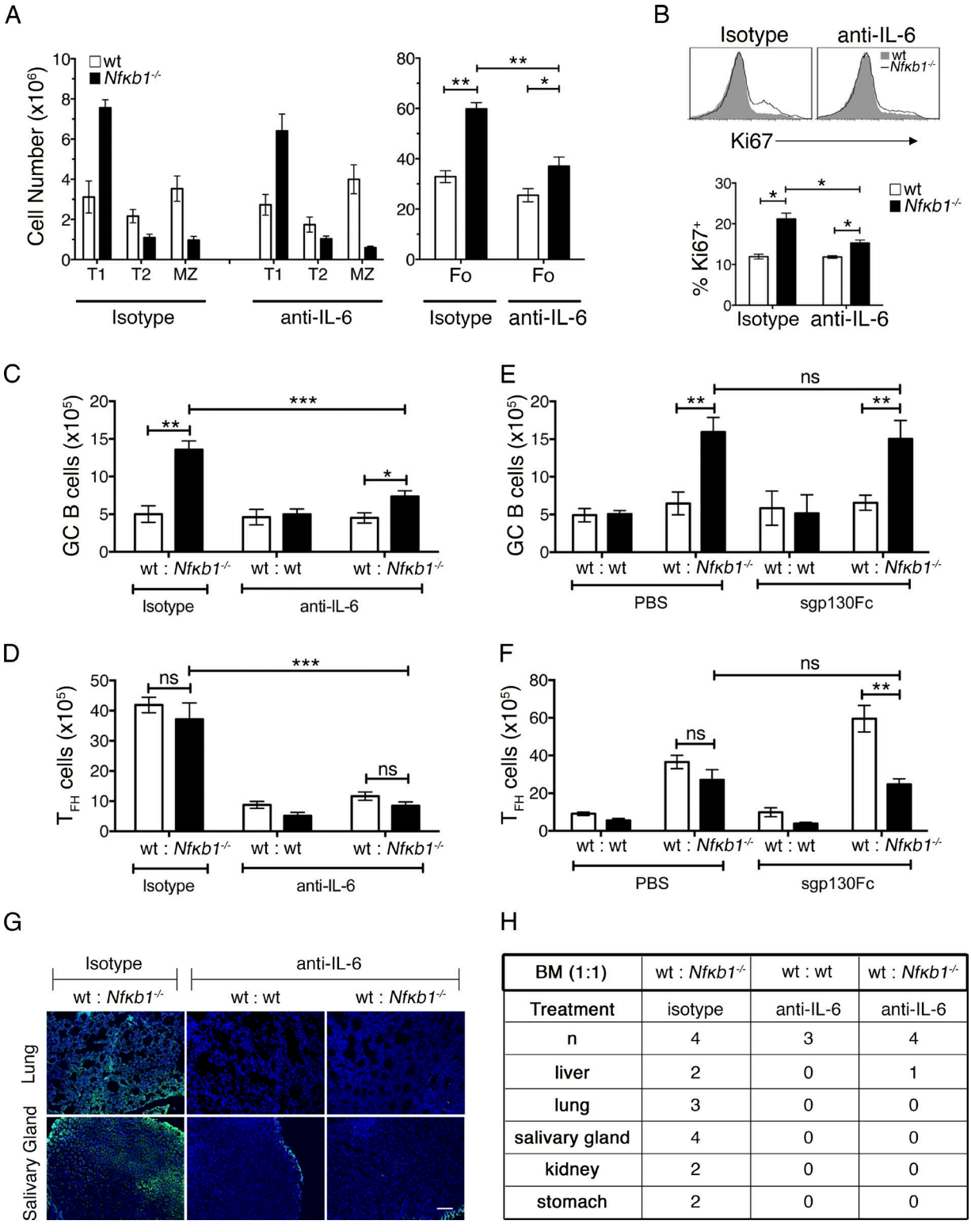

Figure 7. **In vivo neutralization of IL-6 inhibits T_{FH} and GC B cell differentiation.** mBM-reconstituted mice were established as described in Fig. 6. 8 wk after engraftment, control (ly5.1$^+$ WT and ly5.2$^+$ WT) and mutant (ly5.1$^+$ WT and ly5.2$^+$*Nfκb1*$^{-/-}$) mBM chimeras were injected twice per week with anti–IL-6 or an isotype control Ab (both at 10 mg/kg). After 6 wk of treatment, chimeras were euthanized and their spleens were harvested for flow cytometric analysis. (A) Absolute numbers of peripheral B cell subsets from hosts engrafted with WT and *Nfκb1*$^{-/-}$ BM cells. (B) Ki67 expression in WT and *Nfκb1*$^{-/-}$ Fo B cells from mutant mBM chimera mice. Graph shows the percentage of Ki67$^+$ Fo B cells. (C and D) Absolute numbers of GC B cells (C) and T_{FH} cells (D; see

targeted mouse, although the conditional deletion of *c-Rel* and *Rela* in GC B cells revealed that c-REL was required to maintain GC populations, whereas RELA promoted Blimp-1–mediated plasma cell development (Heise et al., 2014).

A recent study using *Nfκb1*^{SSAA} mice that express a mutant form of p105 resistant to IKK-induced proteolysis showed that NFκB1 was required for BCR-induced differentiation of GC B cells and plasma cells (Jacque et al., 2014). Although this mutation had no impact on Fo B cell homeostasis, the IgM and IgG_1 responses to T cell–dependent antigens was impaired, and the spleens lacked GC structures. Similar to our study, the B cell defects were attributed to impaired NFκB1 activity and not Tpl-2–dependent ERK signaling. However, unlike *Nfκb1*$^{-/-}$ mice, which lack both p105 and p50, *Nfκb1*^{SSAA} mice retain p105. Given that p105 functions as an IκB for RELA and c-REL (Savinova et al., 2009), it is conceivable that the loss of p105 in the *Nfκb1*$^{-/-}$ mice leads to enhanced RELA and c-REL activity in B cells that promote chronic disease pathogenesis.

Our findings revealed that in the absence of NFκB1, the BCR and TLR9 activation threshold is reduced and is consistent with NFκB1 being required to limit Fo B cell activation (Shokhirev and Hoffmann, 2013), most notably in a population of proliferating IgM^{hi} *Nfκb1*$^{-/-}$ Fo B cells that produce IL-6. Because Fo B cells were the major source of IL-6 produced in *Nfκb1*$^{-/-}$ mice, we tested whether autocrine/paracrine IL-6/IL-6R signaling influences the antigen responsiveness of not only *Nfκb1*$^{-/-}$ but also WT Fo B cells. Indeed, IL-6 neutralization reduced the increased calcium flux and proliferative response to low-level BCR ligation of *Nfκb1*$^{-/-}$ Fo B cells to near-WT levels. However, WT Fo B cell activation was not enhanced by exposure to IL-6 produced by *Nfκb1*$^{-/-}$ Fo B cells in the mBM chimeras or co-culture assays. When cultured in the presence of exogenous IL-6, this led to the enhanced activation and proliferation of WT Fo B cells to an extent that resembled *Nfκb1*$^{-/-}$ Fo B cells. These findings indicate that autocrine/paracrine IL-6/IL-6R signaling can enhance the activation of *Nfκb1*$^{-/-}$ as well as WT Fo B cells, but unique properties in *Nfκb1*$^{-/-}$ Fo B cells might increase the sensitivity of these cells to IL-6 signaling. Although B cells from young *Nfκb1*$^{-/-}$ mice expressed normal levels of cell surface IL-6R (not depicted), increased IL-6R signaling remains a possibility after BCR ligation.

Elevated IL-6 levels can promote severe immunopathology; this is exemplified by Castleman's disease in humans (Hunter and Jones, 2015). We found that a loss of NFκB1 activity in B cells was sufficient to cause increased systemic levels of IL-6, although it is possible that other cell types contribute to the increased IL-6 levels, particularly at the late stage of pathogenesis in the aging *Nfκb1*$^{-/-}$ mice. IL-6 and IL-21 appear to cooperatively promote T_{FH} and GC B cell differentiation (Karnowski et al., 2012), but an absolute requirement for IL-6 in T_{FH} and GC development remains controversial (Kopf et al., 1998; Nurieva et al., 2008; Poholek et al., 2010). Our finding that blocking IL-6 signaling in mBM-reconstituted mice significantly reduces aberrant T_{FH} and GC B cell differentiation supports a critical role for IL-6 in promoting T_{FH} and GC B cell differentiation, particularly in the absence of NFκB1. Collectively, our findings indicate that NFκB1 negatively regulates classical IL-6/IL-6R signaling during T_{FH} and GC B cell development.

The *Il-6* gene is a direct NFκB target in hematopoietic cells (Libermann and Baltimore, 1990; Matsusaka et al., 1993), yet its detailed cell type and context-specific regulation, including in B lineage cells, remains unclear. After exposure to LPS, IL-6 synthesis appears to first depend on RELA then later on c-REL (Alves et al., 2014). Our findings highlight a previously unrecognized role for p50-NFκB1 in the negative regulation of *Il-6* expression. In naive WT Fo B cells, most p50-NFκB1, but not RELA, was found in the nucleus, with p50-NFκB1 bound to multiple κB motifs in the *Il-6* promoter. The loss of NFκB1 in Fo B cells markedly enhanced the nuclear localization of RELA and increased RELA binding to the κB motifs, which even in the absence of stimulation coincided with the enhanced production of IL-6 in *Nfκb1*$^{-/-}$ Fo B cells. Our data support a model in which p50-NFκB1 homodimers repress *Il-6* transcription in mature Fo B cells, which is consistent with p50-NFκB1 homodimers and histone deactylase 1 being constitutively bound to the *Il-6* promoter in certain cell lines (Zhong et al., 2002; Wilson et al., 2015). However, it remains to be determined whether p105-NFκB1 serves a role in repressing *Il-6* expression in Fo B cells by acting as an IκB-like protein.

In summary, we have examined the roles of NFκB1 in Fo B cell homeostasis and function and found that the loss of NFκB1 leads to the development of aberrant lymphoproliferation and multiorgan autoimmunity in mice. Disease manifestation was primarily the result of NFκB1-deficient Fo B cells producing excessive amounts of IL-6 which, through autocrine/paracrine signaling, resulted in the enhanced differentiation of GC B and T_{FH} cells. We also established that

gating strategy in Fig. S3). Ly5.1$^+$ (white bars) and ly5.2$^+$ (black bars) splenocytes were defined and genotypes shown for each treatment group (x axis). (E and F) At 8 wk, mBM-reconstituted mice were injected twice weekly with 0.5 mg/kg sgp130Fc or vehicle (PBS). Spleens were harvested and analyzed by flow cytometry after 6 wk of treatment. As described in C and D, absolute numbers of GC B cells (E) and T_{FH} cells (F) are shown for each genotype. All data in A–F are shown as the mean ± SEM derived from two independent experiments (n = 4–8 mice/genotype). Statistical significance was determined using independent or paired samples Student's t tests. *, $P < 0.05$; **, $P < 0.001$; ***, $P < 0.0001$. ns, not significant. (G and H) Tissue cryosections from *rag-1/J* mice were subjected to sera from anti–IL-6 or isotype-treated mBM chimera mice, and auto-Abs were detected with FITC goat anti–mouse Ig. (G) Representative images of tissue staining. Bar, 100 μm. (H) Incidence of organ specific auto-Abs, derived from two independent experiments.

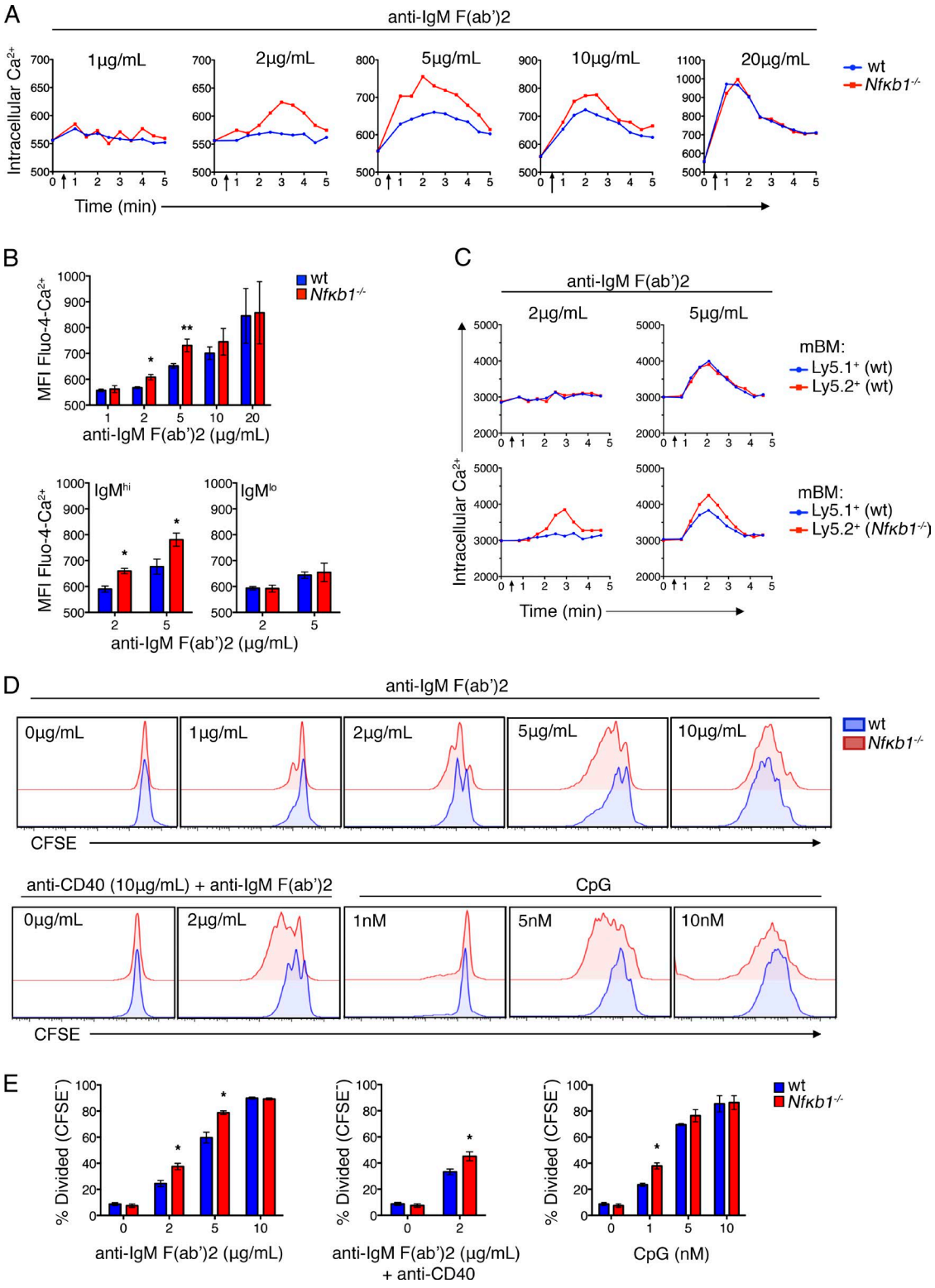

Figure 8. **NFκB1-deficient Fo B cells show increased activation and proliferation in response to BCR and TL9 stimulation.** (A) Relative intracellular Ca^{2+} levels were measured by flow cytometry. Fo B cells were purified from LNs of WT and *Nfκb1*$^{-/-}$ mice (6–8 wk), loaded with Fluo-4 AM and stimulated with graded concentrations of anti-IgM $F(ab')_2$ Ab fragments (added after 30 s; arrows). (B) Graphs show the mean fluorescence intensity (MFI) of Fluo-4 Ca^{2+} in Fo B cells as in A, 2 min after addition of the indicated stimuli: Total Fo B cell population (top), or for IgM^{hi} and IgM^{lo} Fo B cells. (C) Calcium mobilization (as in A) was examined in ly5.1^{+} WT and *Nfκb1*$^{-/-}$ splenic Fo B cells from mBM-reconstituted mice at 14 wk after engraftment (see Fig. 6). (D) Purified

p50-NFκB1 regulates *Il-6* transcription in Fo B cells by restricting RELA-dependent induction. Collectively, these findings demonstrate an essential negative regulatory role for p50-NFκB1 in Fo B cells that prevents the spontaneous generation of autoimmune disease.

MATERIALS AND METHODS

Mouse strains. The *Nfκb1*$^{-/-}$ (Sha et al., 1995) and *Map3k*$^{-/-}$ (Dumitru et al., 2000) mice were originally generated on a mixed C57BL/6 × 129/SV background using 129/SV-derived embryonic stem cells but were backcrossed for more than nine generations onto a C57BL/6 background. All mouse strains, including C57BL/6 (WT), C57BL/6-ly5.1^{+} congenic, *Nfκb1*$^{-/-}$, and *Map3k*$^{-/-}$ mice, were bred and maintained under specific pathogen–free conditions at the Alfred Medical Research and Education Precinct or the Walter and Eliza Hall Institute animal facility. In all aging experiments, the *Nfκb1*$^{-/-}$ mice were from a colony that was maintained on a homozygous-null background and compared with age- and sex-matched C57BL/6 mice. For other experiments, *Nfκb1*$^{+/+}$ and *Nfκb1*$^{-/-}$ littermates were used, which were generated by intercrossing *Nfκb1*$^{+/-}$ heterozygous mice. The generation of BM chimera mice is described in detail in the Generation of BM chimeric mice section. All experiments were conducted under the approval of the respective Animal Ethics Committees of the above institutions and in accordance with National Health and Medical Research Council (NHMRC) Australia guidelines. Mice were provided by P. Tsichlis (Molecular Oncology Research Institute, Tufts Medical Center, Boston, MA).

Cell suspensions and cell counting. Single-cell suspensions were prepared from spleens, LNs, or BM (tibia) using standard protocols. Red blood cells in suspensions from the spleen were lysed by a brief incubation in an ammonium chloride–based lysis buffer containing 0.1 mM EDTA, 150 mM NH_4CL, and 10 mM $NaHCO_3$ in H_2O, pH 7.4. Cell counting was performed using trypan blue dye exclusion and a hemocytometer.

Abs and flow cytometry. Surface staining for flow cytometric analysis was performed using the following fluorochrome-conjugated mAbs: anti–CD19-FITC (1D3), anti–CD24-FITC (M1/69), anti–B220-APCCy7 (RA3-6B2), anti–PD-1–PE (J43), anti–CXCR5-APC (2G8), anti–CD21-APC (7G6), anti–CD45.2-biotin (104), anti–ICOS-biotin (7E.17G9), anti–IgM-biotin (R6-60.2), anti–CD86-FITC (GL1), anti–CD80-PE (16-10A1), anti–MHC class II–biotin (AF6-120.1), anti–IgG1-biotin (A85-1), anti–FAS-biotin (Jo2), anti–CD8-APCCy7 (53-6.7), anti–CD11b-APC (M1/70), and anti–CD3-PE (145-2C11; all from BD); and anti–CD23-FITC, -APC (B3B4), anti-CD4-PE, -biotin (GK1.5), anti–CD45.1-APC, -FITC (A20), anti–CD40-biotin (1C10), and anti–GL7-eFluor660 (GL-7; all from eBioscience). Biotinylated Abs were detected by incubation with steptavidin-PE or -PECy7 (eBioscience).

For intracellular staining, cells were fixed and permeabilized using the Foxp3 Staining Buffer Set (eBioscience) and incubated for 1 h with Alexa Fluor 488–anti-Bcl6 (K112-91; BD) or Alexa Fluor 647–anti-Ki67 (B56; BD). For intracellular cytokine staining, spleen cells were cultured with GolgiStop (BD) for 5 h at 37°C, surface stained, fixed, and permeabilized using the Biosciences Cytofix/Cytoperm Plus Fixation/Permeabilization kit (BD) and then stained with PE-conjugated anti–IL-6 Ab (MP5-20F3; BD). Cell samples were analyzed in FACSCaliber, LSR II, or FACSCanto II flow cytometers (BD) with a minimum of 30,000 events acquired per sample. Data were analyzed using CellQuest Pro (BD) or FlowJo (Tree Star) software. Forward and side scatter light profiles were used to exclude erythrocytes and cell debris, and viable cells were identified by exclusion of propidium iodide.

Histology and immunofluorescence staining of tissues. Organs were fixed in 10% neutral buffered formalin, and 3-µm sections were stained with H&E. Immunofluorescence staining was performed on 5–7-µm optical cutting temperature compound–embedded frozen tissue sections. After acetone fixation, sections were incubated with 10% normal goat serum to block nonspecific binding of Ig. Primary staining was performed using rat anti–mouse B220 (RA3-6B2; eBioscience), IL-6 (MP5-20F3; Bio X Cell), or peanut agglutinin (Vector Laboratories). Bound biotinylated Abs or lectin was detected by staining with Texas red–conjugated Streptavidin (Invitrogen) or Alexa Fluor 488–conjugated goat anti–rat IgG(H+L) Abs (Molecular Probes). Bright-field and fluorescence images were captured on a microscope (BX51 or IX51; Olympus) equipped with a camera (NP70; Olympus). Image analysis was performed using ImageJ software (National Institutes of Health).

Auto-Ab detection by indirect immunofluorescence staining. Screening for auto-Abs in sera was performed by indirect immunofluorescence staining of frozen tissue sections (Mason et al., 2013). To avoid background staining, organs were harvested from 8-wk-old RAG-1/J mice, which lack endogenous Ig. 5-µm tissue sections were fixed in 100% acetone for 10 min and then incubated with mouse sera diluted in PBS. Bound auto-Abs were detected by secondary staining with FITC-conjugated goat anti–mouse IgM, IgA, and IgG Abs (Cappel) and counterstained with DAPI (Sigma-Aldrich). Sections were viewed on a confocal microscope

WT or *Nfκb1*$^{-/-}$ Fo B cells were labeled with CFSE and cultured in the presence of IgM F(ab')$_2$ Ab fragments plus or minus anti-CD40 or CpG. Cell division was measured by CFSE dilution at 72 h. (E) Percentage of divided (CFSE^{-}) cells at 72 h. Data are from three (A, B, D, and E) or two (C) individual experiment ($n \geq 6$ mice/group). Graphs show the mean ± SEM. *, $P < 0.05$, **, $P < 0.001$, determined by unpaired Student's *t* tests.

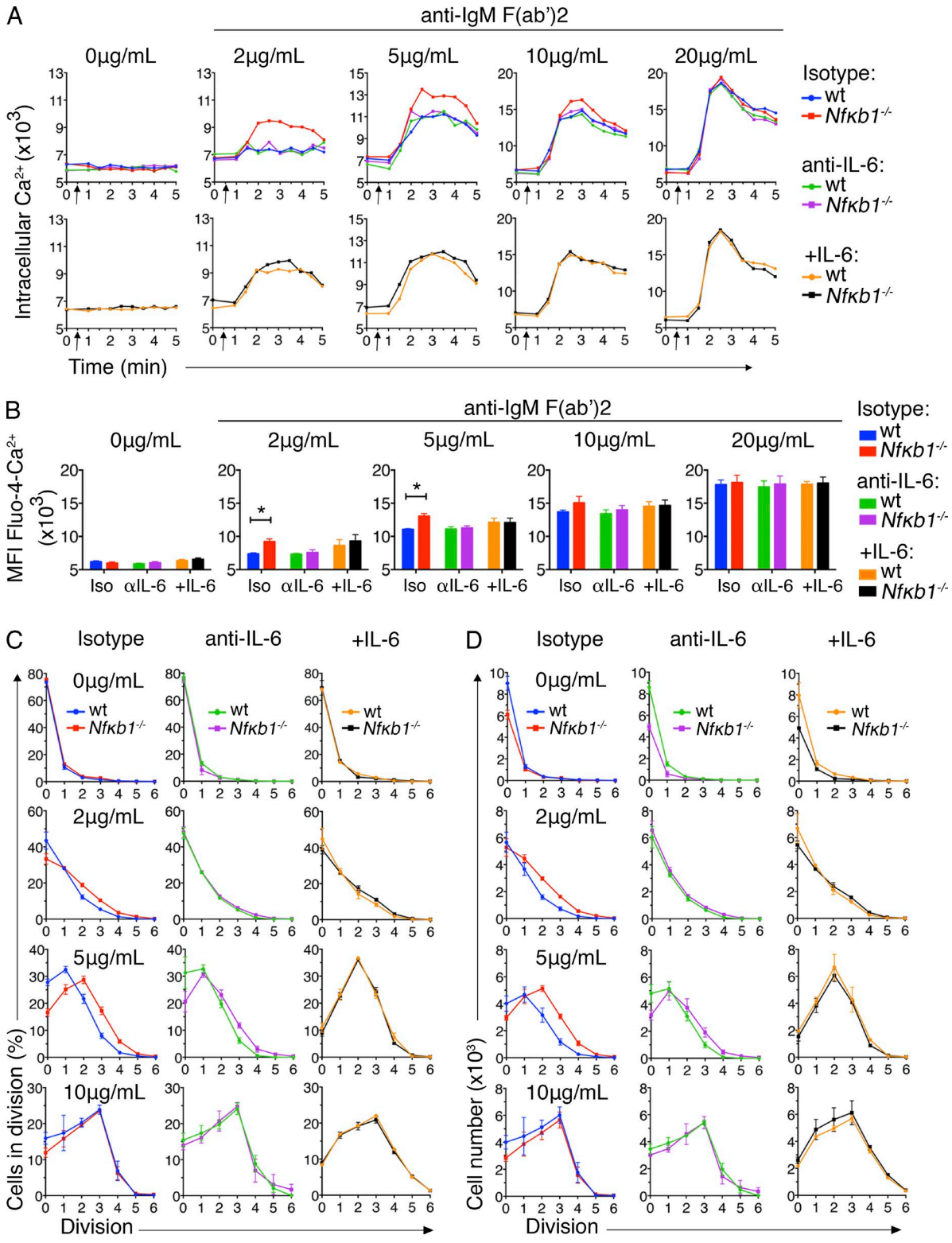

Figure 9. **Autocrine IL-6 signaling causes enhanced sensitivity of NFκB1-deficient Fo B cells.** Fo B cells were purified from LNs of ly5.1$^+$ WT and *Nfκb1*$^{-/-}$ mice (6–8 wk), mixed equally (1:1), and cultured in the presence of anti–IL-6 or isotype control Ab (both at 10 µg/ml). For the addition of exogenous IL-6, B cells were precleared of endogenous IL-6 by incubation with 10 µg/ml anti–IL-6 Ab for 1 h and then cultured with 10 ng/ml IL-6. B cell cultures were stimulated with graded concentrations of anti–IgM F(ab')$_2$ Ab fragments then examined by flow cytometry. (A) Intracellular Ca^{2+} levels were measured in ly5.1$^+$ WT and *Nfκb1*$^{-/-}$ Fo B cells as in Fig 8 A; genotypes were defined by ly5 expression. (B) Graphs show the mean fluorescence intensity (MFI) of Fluo-4

(DIMIRE2; Leica) and assessed for the presence of positive auto-Ab staining.

Cell isolation and tissue culture. B cells were purified (>98% purity) by negative selection using the mouse B cell enrichment kit (EasySep; STEMCELL Technologies). For cell culture assays, B cells were seeded at 5×10^5 cells per well in RPMI + GlutaMAX (Gibco) supplemented with 10% FCS (In Vitro Technologies), 100 U/ml penicillin/streptomycin (Gibco), and 50 μM 2-mercaptoethanol. For stimulation assays, B cells were cultured in graded concentrations of CpG (Invitrogen) and $F(ab')_2$ anti–mouse IgM Ab fragments (Jackson ImmunoResearch Laboratories, Inc.) with or without 10 ng/ml anti-CD40 Ab (IC10) at 37°C (5% CO_2). For in vitro IL-6 neutralization, cultured cells were incubated with 10 ng/ml anti–IL-6 Ab (MP5-20F3; Bio X Cell). However, cultures with exogenous IL-6 were precleared by incubation with 10 μg/ml anti–IL-6 Ab for 1 h before the addition of 10 ng/ml mIL-6 (R&D Systems).

Calcium flux and cell proliferation assays. Purified B cells were loaded for 30 min at room temperature with the fluorescent calcium indicator Fluo-4 AM (Molecular Probes) at 1 μM in HBSS solution. For IL-6 neutralization, cells were preincubated with 10 ng/ml anti–IL-6 Ab for 1 h at 37°C. Cells were analyzed on a FACSCanto II for 30 s to establish a baseline of intracellular calcium levels, briefly removed from the FACS machine, and stimulated as indicated. Cells were then vortexed and immediately placed back on the FACS machine, and intracellular calcium concentration was analyzed for a further 4 min. Calcium flux was assessed by measuring changes in fluorescence of the Fluo-4 dye (520 nm) over time, and kinetic analysis was performed using FlowJo software. For proliferation assays, cells were labeled with 2.5 μM CFSE (Invitrogen) and CFSE dilution (a consequence of cell division) assessed over time in a FACSCanto II flow cytometer. Forward and side light scatter profiles as well as propidium iodide staining were monitored to evaluate the extent of cell death. Cell numbers in each division generation were determined using FlowJo software.

ELISA. ANAs were examined by ELISA. Plates precoated with purified nuclear antigens (The Binding Site Ltd) were incubated with dilutions of mouse sera, and bound Abs were detected by secondary staining with HRP-conjugated goat anti–mouse IgG or Ig(H+L) Abs (SouthernBiotech) followed by the addition of TBM substrate. The reactions were stopped by the addition of 3 M phosphoric acid, and optical density was read at 450 nm with a reference filter of 595 nm. Total serum Ig levels were measured as previously described (O'Reilly et al., 2009). Maxisorp ELISA plates (Thermo Fisher Scientific) were coated with 50 μl/well of captured Abs at 2 μg/ml (goat anti–mouse Ig[H+L] Ab). Serum samples were diluted in a blocking solution (4% skim milk powder and 0.1% Tween-20 in PBS), and myeloma-derived Abs (SouthernBiotech) were used to generate a standard calibration curve. Alkaline phosphatase–conjugated secondary Abs against mouse IgM, IgG, IgA, or IgE (SouthernBiotech) were used at 0.5 μg/ml in a blocking solution, and reactions were developed using 1 mg/ml ABTS (Sigma-Aldrich) in a P-NPP substrate buffer (1 M diethanolamine [0.5 mM $MgCl_2$, pH 9.8]). Optical density was read at 405 nm with a reference filter of 490 nm.

Cytokine bead array. Cytokine concentrations in sera or cell culture supernatants were determined using a multiplex cytometric bead array. The mouse Th1/Th2/Th17/Th22 13-plex FlowCytomix Multiplex kit (BMS822FF; eBioscience) was used according to the manufacturer's instructions. In brief, samples or serial dilutions of cytokine standards were incubated with fluorescent cytokine capture beads and biotin-conjugated anticytokine Abs. Captured cytokines were detected by incubation with PE-conjugated streptavidin. Samples were analyzed on a flow cytometer (FACSCanto II), and data were processed using FlowCytomix Pro 3.0 software (eBioscience).

Nuclear translocation analysis using ImageStream. Cells were fixed (Lyse/Fix buffer; BD), stained for cell type–specific surface markers, permeabilized in Perm buffer III (BD), and then stained intracellularly with Abs against p50-NFκB1 or p65/RelA (Abcam). Staining was detected with Alexa Fluor 488–conjugated secondary anti–rabbit Ig(H+L) Abs (Invitrogen). 5 μM of nuclear dye (Vybrant DyeCycle violet; Invitrogen) was added before the analysis. Fluorescent images were viewed on an Amnis ImageStream 100 imaging flow cytometer (EMD Millipore) with a minimum of 10,000 events acquired per sample. A mask on the nucleus was created, and colocalization of transcription factors and nuclear dye was measured by overlap within this area using Amnis IDEAS software (EMD Millipore).

Generation of BM chimeric mice. BM chimeric mice were generated as previously described (Gugasyan et al., 2012). BM cells were flushed from the femora and tibiae of ly5.2$^+$ WT, *Nfkb1*$^{-/-}$, or *Map3k8*$^{-/-}$ donor mice, and 1–2 × 10^6 BM cells were injected i.v. into lethally irradiated (2 × 550 rads; 3 h apart) ly5.1$^+$ WT or *Nfkb1*$^{-/-}$ hosts. mBM chimeric mice

Ca^{2+} in Fo B cells from A (top) 2 min after the addition of the indicated stimuli. (C and D) Percentage of divided ($CFSE^-$) cells (C) and absolute numbers of WT and *Nfkb1*$^{-/-}$ Fo B cells (D) per cell division peak. WT and *Nfkb1*$^{-/-}$ Fo B cells were labeled with CFSE and cultured as described in Fig. 8 for 72 h. Cell division was assessed by dilution of CFSE (gating strategies are shown in Fig. S4). Data are from two independent experiments (n = 5 mice/genotype). Graphs in B–D show mean ± SEM. *, $P < 0.05$, determined by unpaired Student's t tests.

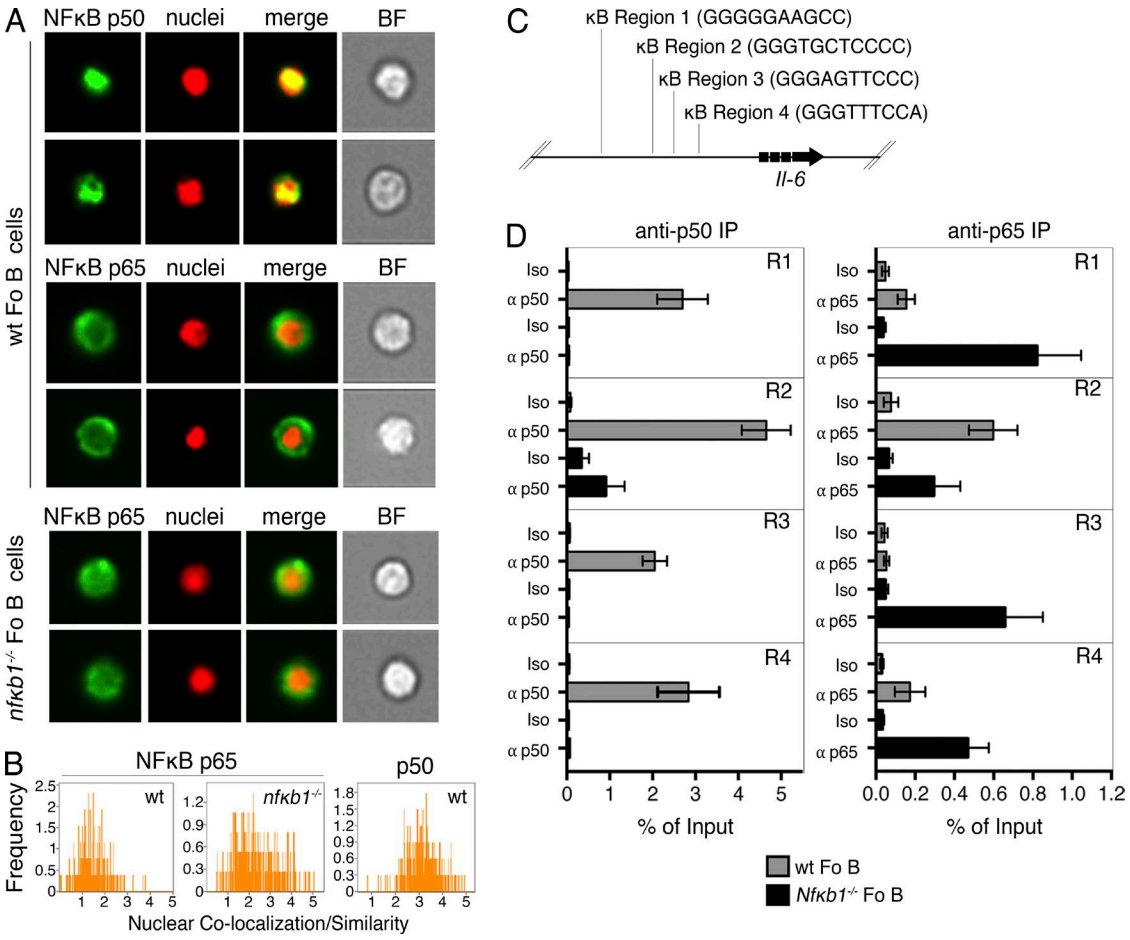

Figure 10. **p50-NFκB1 is a direct negative regulator of the *Il-6* gene in Fo B cells.** (A) Nuclear/cytoplasmic translocation of p50-NFκB1 and p65/RelA was examined by Amnis ImageStream. Images show p65/RelA or p50-NFκB1 combined with a nuclear dye in WT and *Nfκb1*$^{-/-}$ Fo B cells (B220^{+}CD21^{int}IgM^{lo}). (B) Relative colocalization of p65/RelA or p50-NFκB1 with the nuclear dye in Fo B cells. (C and D) ChIP was performed on purified Fo B cells from WT and *Nfκb1*$^{-/-}$ mice with an anti-p50, anti-p65/RelA, or isotype control Ab. (C) Schematic representation of four putative p50-NFκB1–binding sites in the *Il-6* promoter. (D) Enrichment of *Il-6* κB regions 1–4 as measured by qPCR (mean ± SEM). Data are from two to four independent experiments ($n \geq 4$ mice/genotype).

were established by injecting lethally irradiated ly5.1^{+} WT hosts with an equal mix (1:1) of BM cells from either ly5.1^{+} WT and *Nfκb1*$^{-/-}$ or ly5.1^{+} and ly5.2^{+} WT donor mice. All host mice were maintained on antibiotic water (Neomycin) for 6 wk and acidified drinking water thereafter.

IL-6 neutralization. For IL-6–blocking experiments, mBM chimeric mice were randomly assigned to treatment groups 8 wk after engraftment. To neutralize IL-6 in vivo, chimeras were injected i.p twice weekly with anti–IL-6 Ab (clone MP5-20F3, rat IgG1; Bio X Cell) or an Ig isotype–matched control mAb (both at 10 mg/kg body weight; anti–rat IgG1; Bio X Cell). To disrupt trans–IL-6 signaling, chimeras were injected i.p twice weekly with 0.5 mg/kg body weight–soluble gp130Fc protein (CONARIS; Schuett et al., 2012) or vehicle (PBS). All mice were euthanized and analyzed after 6 wk of treatment.

Quantitative PCR (qPCR) array. RNA was isolated from cells using the RNeasy Mini kit (QIAGEN). Total RNA was reverse transcribed using the RT^2 First Strand cDNA kit (QIAGEN), and the levels of 84 autoimmune and inflammatory immune response genes were analyzed using the RT^2 Profiler PCR Array (Format E; PAMM-077Z; QIAGEN) according to the manufacturer's instructions.

ChIP. ChIP was performed on 6 × 10^7 purified B cells according to the manufacturer's guidelines (EMD Millipore). Cells were fixed for 10 min in 1% paraformaldehyde, quenched with glycine (EMD Millipore), and washed in ice-cold PBS. DNA was fragmented by sonication for 45 cycles of 30 s each at the maximum speed using a Bio-Ruptor 4000 (OMNI International Inc). Immunoprecipitation was performed with 10 µg ChIP-grade Abs against p50-NFκB1 or p65/RelA (both from Abcam) or an equivalent amount of

rabbit IgG as a negative control. To measure enrichment, qPCR was performed with the primers listed in Table S1. Reactions were performed in triplicate with SYBR green PCR master mix (QIAGEN) on an ABI 7800HT machine (Applied Biosystems).

Statistical analysis. The graphing and statistical analysis of data was performed using Prism (GraphPad Software), and statistical significance was determined using independent or paired-sample Student's *t* tests. All data are presented as mean ± SEM, and differences are considered statistically significant if $P < 0.05$.

Online supplemental material. Fig. S1 shows gating strategies for Fig. 1. Fig. S2 shows gating strategies for Fig. 3. Fig. S3 shows gating strategies for Fig. 7. Fig. S4 shows gating strategies for Fig. 9. Table S1 lists the primers used for qPCR of ChIP DNA. Online supplemental material is available at http://www.jem.org/cgi/content/full/jem.20151182/DC1.

ACKNOWLEDGMENTS

We thank Alfred Medical Research and Education Precinct Micro Imaging and Flow Cytometry Services of Monash University, the Materials Characterization and Fabrication Platform of the University of Melbourne, Dr. Philip Tsichlis for the *Map3k*$^{-/-}$ mice, and Dr. Wei Shi and Ms. Ann Lin for technical assistance.

This work was funded by the National Health and Medical Research Council (NHMRC) of Australia as follows: a fellowship to A. Strasser (1020363); a program grant to A. Strasser (1016701); and project grants to L.A. O'Reilly (1009145), M.L. Hibbs (1008288), A. Strasser (1046010), and R. Gugasyan (603713). E. de Valle is a recipient of an Australian Postgraduate Award. G. Grigoriadis is supported by a Haematology Society of Australia and New Zealand (HSANZ) New/Young Investigator Award and is a Victorian Cancer Agency Clinical Research fellow. A. Kallies is supported by the Sylvia and Charles Viertel Foundation. We gratefully acknowledge the Victorian Operational Infrastructure Support Program and an NHMRC infrastructure grant.

The authors declare no competing financial interests.

Submitted: 20 July 2015

Accepted: 1 March 2016

REFERENCES

Alves, B.N., R. Tsui, J. Almaden, M.N. Shokhirev, J. Davis-Turak, J. Fujimoto, H. Birnbaum, J. Ponomarenko, and A. Hoffmann. 2014. IκBε is a key regulator of B cell expansion by providing negative feedback on cRel and RelA in a stimulus-specific manner. *J. Immunol.* 192:3121–3132. http://dx.doi.org/10.4049/jimmunol.1302351

Banerjee, A., R. Grumont, R. Gugasyan, C. White, A. Strasser, and S. Gerondakis. 2008. NF-κB1 and c-Rel cooperate to promote the survival of TLR4-activated B cells by neutralizing Bim via distinct mechanisms. *Blood.* 112:5063–5073. http://dx.doi.org/10.1182/blood-2007-10-120832

Basso, K., and R. Dalla-Favera. 2012. Roles of BCL6 in normal and transformed germinal center B cells. *Immunol. Rev.* 247:172–183. http://dx.doi.org/10.1111/j.1600-065X.2012.01112.x

Basso, K., U. Klein, H. Niu, G.A. Stolovitzky, Y. Tu, A. Califano, G. Cattoretti, and R. Dalla-Favera. 2004. Tracking CD40 signaling during germinal center development. *Blood.* 104:4088–4096. http://dx.doi.org/10.1182/blood-2003-12-4291

Beinke, S., J. Deka, V. Lang, M.P. Belich, P.A. Walker, S. Howell, S.J. Smerdon, S.J. Gamblin, and S.C. Ley. 2003. NF-κB1 p105 negatively regulates TPL-2 MEK kinase activity. *Mol. Cell. Biol.* 23:4739–4752. http://dx.doi.org/10.1128/MCB.23.14.4739-4752.2003

Bernal, G.M., J.S. Wahlstrom, C.D. Crawley, K.E. Cahill, P. Pytel, H. Liang, S. Kang, R.R. Weichselbaum, and B. Yamini. 2014. Loss of *Nfkb1* leads to early onset aging. *Aging (Albany, N.Y.).* 6:931–943.

Burkitt, M.D., J.M. Williams, C.A. Duckworth, A. O'Hara, A. Hanedi, A. Varro, J.H. Caamaño, and D.M. Pritchard. 2013. Signaling mediated by the NF-κB sub-units NF-κB1, NF-κB2 and c-Rel differentially regulate Helicobacter felis-induced gastric carcinogenesis in C57BL/6 mice. *Oncogene.* 32:5563–5573. http://dx.doi.org/10.1038/onc.2013.334

Cariappa, A., H.C. Liou, B.H. Horwitz, and S. Pillai. 2000. Nuclear factor κb is required for the development of marginal zone B lymphocytes. *J. Exp. Med.* 192:1175–1182. http://dx.doi.org/10.1084/jem.192.8.1175

Cheng, S., C.Y. Hsia, G. Leone, and H.C. Liou. 2003. Cyclin E and Bcl-x_L cooperatively induce cell cycle progression in c-Rel$^{-/-}$ B cells. *Oncogene.* 22:8472–8486. http://dx.doi.org/10.1038/sj.onc.1206917

Claudio, E., K. Brown, S. Park, H. Wang, and U. Siebenlist. 2002. BAFF-induced NEMO-independent processing of NF-κB2 in maturing B cells. *Nat. Immunol.* 3:958–965. http://dx.doi.org/10.1038/ni842

Crotty, S. 2011. Follicular helper CD4 T cells (TFH). *Annu. Rev. Immunol.* 29:621–663. http://dx.doi.org/10.1146/annurev-immunol-031210-101400

de Valle, E., L.K. Lie, S.P. Berzins, and R. Gugasyan. 2012. The role of NFkB in T-lymphocyte development and function. *J. Clin. Cell. Immunol.* S12:009. http://dx.doi.org/10.4172/2155-9899.S12-009

Dumitru, C.D., J.D. Ceci, C. Tsatsanis, D. Kontoyiannis, K. Stamatakis, J.H. Lin, C. Patriotis, N.A. Jenkins, N.G. Copeland, G. Kollias, and P.N. Tsichlis. 2000. TNF-α induction by LPS is regulated posttranscriptionally via a Tpl2/ERK-dependent pathway. *Cell.* 103:1071–1083. http://dx.doi.org/10.1016/S0092-8674(00)00210-5

Erdman, S.E., J.G. Fox, C.A. Dangler, D. Feldman, and B.H. Horwitz. 2001. Cutting edge: Typhlocolitis in NF-κB-deficient mice. *J. Immunol.* 166:1443–1447. http://dx.doi.org/10.4049/jimmunol.166.3.1443

Gerondakis, S., and U. Siebenlist. 2010. Roles of the NF-κB pathway in lymphocyte development and function. *Cold Spring Harb. Perspect. Biol.* 2:a000182. http://dx.doi.org/10.1101/cshperspect.a000182

Grumont, R.J., and S. Gerondakis. 1994. The subunit composition of NF-κB complexes changes during B-cell development. *Cell Growth Differ.* 5:1321–1331.

Grumont, R.J., I.J. Rourke, L.A. O'Reilly, A. Strasser, K. Miyake, W. Sha, and S. Gerondakis. 1998. B lymphocytes differentially use the Rel and nuclear factor κB1 (NF-κB1) transcription factors to regulate cell cycle progression and apoptosis in quiescent and mitogen-activated cells. *J. Exp. Med.* 187:663–674. http://dx.doi.org/10.1084/jem.187.5.663

Grumont, R.J., A. Strasser, and S. Gerondakis. 2002. B cell growth is controlled by phosphatidylinosotol 3-kinase-dependent induction of Rel/NF-κB regulated c-myc transcription. *Mol. Cell.* 10:1283–1294. http://dx.doi.org/10.1016/S1097-2765(02)00779-7

Gugasyan, R., E. Horat, S.A. Kinkel, F. Ross, G. Grigoriadis, D. Gray, M. O'Keeffe, S.P. Berzins, G.T. Belz, R.J. Grumont, et al. 2012. The NF-κB1 transcription factor prevents the intrathymic development of CD8 T cells with memory properties. *EMBO J.* 31:692–706. http://dx.doi.org/10.1038/emboj.2011.435

Hayden, M.S., and S. Ghosh. 2011. NF-κB in immunobiology. *Cell Res.* 21:223–244. http://dx.doi.org/10.1038/cr.2011.13

Heise, N., N.S. De Silva, K. Silva, A. Carette, G. Simonetti, M. Pasparakis, and U. Klein. 2014. Germinal center B cell maintenance and differentiation are controlled by distinct NF-κB transcription factor subunits. *J. Exp. Med.* 211:2103–2118. http://dx.doi.org/10.1084/jem.20132613

Hunter, C.A., and S.A. Jones. 2015. IL-6 as a keystone cytokine in health and disease. *Nat. Immunol.* 16:448–457. http://dx.doi.org/10.1038/ni.3153

Jacque, E., E. Schweighoffer, A. Visekruna, S. Papoutsopoulou, J. Janzen, R. Zillwood, D.M. Tarlinton, V.L. Tybulewicz, and S.C. Ley. 2014. IKK-induced NF-κB1 p105 proteolysis is critical for B cell antibody responses to T cell-dependent antigen. *J. Exp. Med.* 211:2085–2101. http://dx.doi.org/10.1084/jem.20132019

Jurk, D., C. Wilson, J.F. Passos, F. Oakley, C. Correia-Melo, L. Greaves, G. Saretzki, C. Fox, C. Lawless, R. Anderson, et al. 2014. Chronic inflammation induces telomere dysfunction and accelerates ageing in mice. *Nat. Commun.* 2:4172. http://dx.doi.org/10.1038/ncomms5172

Kaileh, M., and R. Sen. 2012. NF-κB function in B lymphocytes. *Immunol. Rev.* 246:254–271. http://dx.doi.org/10.1111/j.1600-065X.2012.01106.x

Karnowski, A., S. Chevrier, G.T. Belz, A. Mount, D. Emslie, K. D'Costa, D.M. Tarlinton, A. Kallies, and L.M. Corcoran. 2012. B and T cells collaborate in antiviral responses via IL-6, IL-21, and transcriptional activator and coactivator, Oct2 and OBF-1. *J. Exp. Med.* 209:2049–2064. http://dx.doi.org/10.1084/jem.20111504

Klein, U., and R. Dalla-Favera. 2008. Germinal centres: role in B-cell physiology and malignancy. *Nat. Rev. Immunol.* 8:22–33. http://dx.doi.org/10.1038/nri2217

Kopf, M., S. Herren, M.V. Wiles, M.B. Pepys, and M.H. Kosco-Vilbois. 1998. Interleukin 6 influences germinal center development and antibody production via a contribution of C3 complement component. *J. Exp. Med.* 188:1895–1906. http://dx.doi.org/10.1084/jem.188.10.1895

Li, Z.W., S.A. Omori, T. Labuda, M. Karin, and R.C. Rickert. 2003. IKKβ is required for peripheral B cell survival and proliferation. *J. Immunol.* 170:4630–4637. http://dx.doi.org/10.4049/jimmunol.170.9.4630

Libermann, T.A., and D. Baltimore. 1990. Activation of interleukin-6 gene expression through the NF-kappa B transcription factor. *Mol. Cell. Biol.* 10:2327–2334. http://dx.doi.org/10.1128/MCB.10.5.2327

Mason, K.D., A. Lin, L. Robb, E.C. Josefsson, K.J. Henley, D.H. Gray, B.T. Kile, A.W. Roberts, A. Strasser, D.C. Huang, et al. 2013. Proapoptotic Bak and Bax guard against fatal systemic and organ-specific autoimmune disease. *Proc. Natl. Acad. Sci. USA.* 110:2599–2604. http://dx.doi.org/10.1073/pnas.1215097110

Matsusaka, T., K. Fujikawa, Y. Nishio, N. Mukaida, K. Matsushima, T. Kishimoto, and S. Akira. 1993. Transcription factors NF-IL6 and NF-kappa B synergistically activate transcription of the inflammatory cytokines, interleukin 6 and interleukin 8. *Proc. Natl. Acad. Sci. USA.* 90:10193–10197. http://dx.doi.org/10.1073/pnas.90.21.10193

Nurieva, R.I., Y. Chung, D. Hwang, X.O. Yang, H.S. Kang, L. Ma, Y.H. Wang, S.S. Watowich, A.M. Jetten, Q. Tian, and C. Dong. 2008. Generation of T follicular helper cells is mediated by interleukin-21 but independent of T helper 1, 2, or 17 cell lineages. *Immunity.* 29:138–149. http://dx.doi.org/10.1016/j.immuni.2008.05.009

O'Reilly, L.A., L. Tai, L. Lee, E.A. Kruse, S. Grabow, W.D. Fairlie, N.M. Haynes, D.M. Tarlinton, J.G. Zhang, G.T. Belz, et al. 2009. Membrane-bound Fas ligand only is essential for Fas-induced apoptosis. *Nature.* 461:659–663. http://dx.doi.org/10.1038/nature08402

Oakley, F., J. Mann, S. Nailard, D.E. Smart, N. Mungalsingh, C. Constandinou, S. Ali, S.J. Wilson, H. Millward-Sadler, J.P. Iredale, and D.A. Mann. 2005. Nuclear factor-κB1 (p50) limits the inflammatory and fibrogenic responses to chronic injury. *Am. J. Pathol.* 166:695–708. http://dx.doi.org/10.1016/S0002-9440(10)62291-2

Pasparakis, M., M. Schmidt-Supprian, and K. Rajewsky. 2002. IκB kinase signaling is essential for maintenance of mature B cells. *J. Exp. Med.* 196:743–752. http://dx.doi.org/10.1084/jem.20020907

Pillai, S., H. Mattoo, and A. Cariappa. 2011. B cells and autoimmunity. *Curr. Opin. Immunol.* 23:721–731. http://dx.doi.org/10.1016/j.coi.2011.10.007

Pohl, T., R. Gugasyan, R.J. Grumont, A. Strasser, D. Metcalf, D. Tarlinton, W. Sha, D. Baltimore, and S. Gerondakis. 2002. The combined absence of NF-κB1 and c-Rel reveals that overlapping roles for these transcription factors in the B cell lineage are restricted to the activation and function of mature cells. *Proc. Natl. Acad. Sci. USA.* 99:4514–4519. http://dx.doi.org/10.1073/pnas.072071599

Poholek, A.C., K. Hansen, S.G. Hernandez, D. Eto, A. Chandele, J.S. Weinstein, X. Dong, J.M. Odegard, S.M. Kaech, A.L. Dent, et al. 2010. In vivo regulation of Bcl6 and T follicular helper cell development. *J. Immunol.* 185:313–326. http://dx.doi.org/10.4049/jimmunol.0904023

Rose-John, S. 2012. IL-6 trans-signaling via the soluble IL-6 receptor: importance for the pro-inflammatory activities of IL-6. *Int. J. Biol. Sci.* 8:1237–1247. http://dx.doi.org/10.7150/ijbs.4989

Savinova, O.V., A. Hoffmann, and G. Ghosh. 2009. The Nfkb1 and Nfkb2 proteins p105 and p100 function as the core of high-molecular-weight heterogeneous complexes. *Mol. Cell.* 34:591–602. http://dx.doi.org/10.1016/j.molcel.2009.04.033

Schuett, H., R. Oestreich, G.H. Waetzig, W. Annema, M. Luchtefeld, A. Hillmer, U. Bavendiek, J. von Felden, D. Divchev, T. Kempf, et al. 2012. Transsignaling of interleukin-6 crucially contributes to atherosclerosis in mice. *Arterioscler. Thromb. Vasc. Biol.* 32:281–290. http://dx.doi.org/10.1161/ATVBAHA.111.229435

Sha, W.C., H.C. Liou, E.I. Tuomanen, and D. Baltimore. 1995. Targeted disruption of the p50 subunit of NF-κB leads to multifocal defects in immune responses. *Cell.* 80:321–330. http://dx.doi.org/10.1016/0092-8674(95)90415-8

Shaffer, A.L. III, R.M. Young, and L.M. Staudt. 2012. Pathogenesis of human B cell lymphomas. *Annu. Rev. Immunol.* 30:565–610. http://dx.doi.org/10.1146/annurev-immunol-020711-075027

Shokhirev, M.N., and A. Hoffmann. 2013. FlowMax: A computational tool for maximum likelihood deconvolution of CFSE time courses. *PLoS One.* 8:e67620. http://dx.doi.org/10.1371/journal.pone.0067620

Snapper, C.M., P. Zelazowski, F.R. Rosas, M.R. Kehry, M. Tian, D. Baltimore, and W.C. Sha. 1996. B cells from p50/NF-kappa B knockout mice have selective defects in proliferation, differentiation, germ-line CH transcription, and Ig class switching. *J. Immunol.* 156:183–191.

Ueno, H., J. Banchereau, and C.G. Vinuesa. 2015. Pathophysiology of T follicular helper cells in humans and mice. *Nat. Immunol.* 16:142–152. http://dx.doi.org/10.1038/ni.3054

Victora, G.D., T.A. Schwickert, D.R. Fooksman, A.O. Kamphorst, M. Meyer-Hermann, M.L. Dustin, and M.C. Nussenzweig. 2010. Germinal center dynamics revealed by multiphoton microscopy with a photoactivatable fluorescent reporter. *Cell.* 143:592–605. http://dx.doi.org/10.1016/j.cell.2010.10.032

Vinuesa, C.G., I. Sanz, and M.C. Cook. 2009. Dysregulation of germinal centres in autoimmune disease. *Nat. Rev. Immunol.* 9:845–857. http://dx.doi.org/10.1038/nri2637

Waterfield, M.R., M. Zhang, L.P. Norman, and S.C. Sun. 2003. NF-κB1/p105 regulates lipopolysaccharide-stimulated MAP kinase signaling by governing the stability and function of the Tpl2 kinase. *Mol. Cell.* 11:685–694. http://dx.doi.org/10.1016/S1097-2765(03)00070-4

Wilson, C.L., D. Jurk, N. Fullard, P. Banks, A. Page, S. Luli, A.M. Elsharkawy, R.G. Gieling, J.B. Chakraborty, C. Fox, et al. 2015. *NFκB1* is a suppressor of neutrophil-driven hepatocellular carcinoma. *Nat. Commun.* 6:6818. http://dx.doi.org/10.1038/ncomms7818

Zhong, H., M.J. May, E. Jimi, and S. Ghosh. 2002. The phosphorylation status of nuclear NF-κB determines its association with CBP/p300 or HDAC-1. *Mol. Cell.* 9:625–636. http://dx.doi.org/10.1016/S1097-2765(02)00477-X